HHS Public Access

Author manuscript

Nat Metab. Author manuscript; available in PMC 2019 September 05.

Published in final edited form as:

Nat Metab. 2019 February ; 1(2): 276–290. doi:10.1038/s42255-018-0023-6.

MANF regulates metabolic and immune homeostasis in ageing and protects against liver damage

Pedro Sousa-Victor[1,7], **Joana Neves**[1], **Wendy Cedron-Craft**[1,7], **P. Britten Ventura**[2,3], **Chen-Yu Liao**[1], **Rebeccah R. Riley**[1], **Ilya Soifer**[5], **Nicholas van Bruggen**[5], **Ganesh A. Kolumam**[5], **Saul A. Villeda**[2,3], **Deepak A. Lamba**[1,3,4], **Heinrich Jasper**[1,6,*]

[1]Paul F. Glenn Center for Biology of Aging Research, Buck Institute for Research on Aging, 8001 Redwood Boulevard, Novato, CA 94945-1400, USA

[2]Department of Anatomy, University of California, San Francisco, San Francisco, USA

[3]The Eli and Edythe Broad Center of Regeneration Medicine and Stem Cell Research, University of California, San Francisco, San Francisco, USA

[4]Department of Ophthalmology, University of California, San Francisco, San Francisco, USA

[5]Calico Life Sciences LLC, 1170 Veterans Blvd, South San Francisco, California 94080, USA

[6]Immunology Discovery, Genentech, Inc., 1 DNA Way, South San Francisco, California 94080, USA.

[7]Equal contribution

Abstract

Aging is accompanied by altered intercellular communication, deregulated metabolic function, and inflammation. Interventions that restore a youthful state delay or reverse these processes, prompting the search for systemic regulators of metabolic and immune homeostasis. Here we identify MANF, a secreted stress-response protein with immune modulatory properties, as an evolutionarily conserved regulator of systemic and in particular liver metabolic homeostasis. We show that MANF levels decline with age in flies, mice and humans, and MANF overexpression extends lifespan in flies. MANF deficient flies exhibit enhanced inflammation and shorter

*Correspondence to: jasperh@gene.com, Phone: +1 650 797 7040.

Author contributions

PSV, JN, DAL and HJ conceived the study. PSV and JN designed and analyzed all experiments. PSV, JN and WCC performed experiments and collected data. PBV and SAV performed and supervised heterochronic parabiosis experiment. RRR and CYL assisted with in vivo mouse experiments. IS performed transcriptomic analysis. GAK and NVB provided human samples, plasmids for HTV experiments and other reagents, provided expertise for experimental design and analysis, and supervised transcriptomic analysis experiments. PSV and JN interpreted the results, prepared the figures and wrote the manuscript, with input from DAL and HJ. DAL and HJ supervised the study. All authors revised the manuscript.

Competing Interests

The Authors declare no competing interests.

Data availability

All the data generated or analyzed during this study are included in the published article and its Supplementary Information files, and are available from the corresponding author. Analyzed RNA-sequencing data are available in Supplementary Table 1 and raw RNA-sequencing data are available under accession numbers GSE123115, GSE123116 and GSE123117 on the NCBI Gene Expression Omnibus database. Correspondence and requests for materials should be addressed to HJ, PSV and JN.

lifespans, and MANF heterozygous mice exhibit inflammatory phenotypes in various tissues, as well as progressive liver damage, fibrosis, and steatosis. We show that immune cell-derived MANF protects against liver inflammation and fibrosis, while hepatocyte-derived MANF prevents hepatosteatosis. Liver rejuvenation by heterochronic parabiosis in mice further depends on MANF, while MANF supplementation ameliorates several hallmarks of liver aging, prevents hepatosteatosis induced by diet, and improves age-related metabolic dysfunction. Our findings identify MANF as a systemic regulator of homeostasis in young animals, suggesting a therapeutic application for MANF in age-related metabolic diseases.

In metazoans, aging is accompanied by a widespread and coordinated functional decline of many tissues. Common, evolutionarily conserved, hallmarks of aging have been proposed as causes as well as consequences of this decline. One such hallmark is the alteration in intercellular communication associated with inflammation[1]. Progressive low-grade chronic inflammation accompanies the aging process, and may be predictive of many age-related diseases[2], yet the origins of this dysfunction remain unclear.

The importance of changes in intercellular communication in causing age-related physiological changes is supported by experimental interventions aimed at restoring a youthful systemic milieu, such as heterochronic parabiosis. Such interventions demonstrate that the modulation of cytokines and circulating factors in elderly individuals can have a significant impact on aging of a wide range of tissues[3,4], including the liver[5,6]. Optimal inflammation management can not only be achieved by changing the concentration of circulating factors, but also by targeting immune cells[7], which can significantly impact the inflammatory tone of a tissue or organ by secreting a large number of inflammatory cytokines. Of particular interest is the ability of immune cells to polarize into states that are distinctly anti-inflammatory, and that promote tissue repair and tissue homeostasis[8], a shift necessary for some of the rejuvenating effects of heterochronic parabiosis[9].

Increased inflammation in aging animals is conserved in invertebrates[10,11]. A well-described example is the fruit fly, where inflammation-induced changes in intestinal homeostasis contribute to mortality as the animal ages. These age-related inflammatory alterations are also tightly correlated with systemic metabolic dysfunction[12], and limiting inflammation is sufficient to extend lifespan[10].

In mammals, chronic age-related inflammation also underlies the systemic deregulation of metabolic function that is linked to obesity, metabolic syndrome and diabetes, and that impacts major metabolic organs, such as the liver[13]. The prevalence of metabolic syndrome and nonalcoholic fatty liver disease (NAFLD), ranging from liver steatosis to non-alcoholic steatohepatitis (NASH), increases with age[14,15] and pharmacologic approaches that reduce inflammation improve liver homeostasis[16]. Highlighting the benefits of inflammation management in the control of metabolic homeostasis, interventions aimed at reducing inflammation are effective in improving glycemic control in patients with type 2 diabetes and are protective against the development of insulin resistance in animal models exposed to metabolic stressors[17,18].

In a recent study, we discovered that Mesencephalic Astrocyte-derived Neurotrophic Factor (MANF) is expressed in immune cells and has an autocrine immune modulatory function, promoting anti-inflammatory activation in both flies and mice. This function of MANF is essential for its neuroprotective and tissue repair promoting activities in the retina[19]. MANF is an evolutionarily conserved protein[20], found in the blood of humans[21,22], and expressed by most tissues in the body[23]. It is induced in response to several stress signals and is cytoprotective in multiple systems[24]. *In vivo*, MANF function has been associated with the resolution of tissue damage and inflammation[19,25–27]. However, how MANF expression is affected by aging, and whether changes in MANF activity itself contribute to inflammation and metabolic dysfunction in aging animals, remains unknown.

Here, we report that systemic levels of MANF decline in aging flies, mice and humans, and that this reduction contributes to the age-related loss of tissue homeostasis in flies and mice. Animals deficient in MANF exhibit progressive liver dysfunction and are impaired in their ability to induce rejuvenation in the old partner during heterochronic parabiosis. These effects are a consequence of MANF derived from immune cells and hepatocytes, as conditional MANF knockout in each cell type can recapitulate different aspects of liver dysfunction. Importantly, restoring MANF levels can extend fly lifespan, reverse liver damage and inflammation in old mice, and prevent the development of hepatosteatosis in high-fat diet conditions. Based on our data we propose that MANF acts as an evolutionarily conserved regulator of metabolic and immune homeostasis with beneficial effects on health in aging animals.

Results

Systemic levels of MANF protein decline with age in flies, mice and humans

To test whether age-related inflammation is associated with a reduction in MANF signalling, we evaluated the levels of MANF protein during normal aging in flies and mice. Whole body levels of MANF protein were significantly reduced in old *Drosophila* (Fig. 1a) and mouse tissue (Fig. 1b, liver, muscle, fat and skin), and plasma levels of MANF protein progressively and significantly declined with age (Fig. 1c). A similar reduction in the circulating levels of MANF was observed in human serum (Fig. 1d), in line with reports of down-regulation of MANF expression in aging human skin[28].

MANF overexpression extends lifespan in flies

We asked whether this change in MANF expression would impact age-related phenotypes and longevity in flies (Fig. 2a-k). Fly aging is accompanied by a decline in intestinal homeostasis, triggered by JAK/STAT mediated metaplasia of the gastric region, which in turn results in intestinal stem cell (ISC) deregulation, epithelial dysplasia, and finally barrier dysfunction, which causes mortality[10,11,29]. When MANF was knocked down ubiquitously, or in immune cells (hemocytes) specifically, we observed a significantly shorter lifespan (Fig. 2a,c,k). This was accompanied by accelerated ISC over-proliferation (increased number of mitotic figures in the gut; Fig. 2b,d) and JAK-STAT activation in the gut (Fig. 2e), similar to what is observed in old flies. Overexpression of inflammatory cytokines in hemocytes mimicked these effects (Supplementary Fig. 1a). Moreover, knocking down

MANF in the fatbody, but not in intestinal enterocytes also resulted in ISC hyperproliferation (Supplementary Fig. 1b).

To ask whether the decline in homeostasis and increase in mortality of wild-type flies may be a consequence of reduced MANF expression in old flies, we overexpressed MANF in a variety of tissues and assessed lifespan and intestinal homeostasis in these animals. MANF overexpression in fatbody and hemocytes, as well as gut enterocytes, significantly reduced the number of mitotic ISCs in the gut of old animals (Fig. 2f). This was accompanied by a reduction in the expression of the inflammatory cytokine Upd3 (Fig. 2g), indicating that the expression of MANF prevents age-related inflammation and the loss of epithelial homeostasis.

We found that overexpression of MANF in the fatbody or hemocytes resulted in significant mean and maximum lifespan extension (Fig. 2h,i,k). Moreover, expression of MANF from cells/tissues in which Upd3 is induced resulted in strong and significant extension of mean and maximum lifespan (Fig. 2j,k), suggesting that the anti-inflammatory role of MANF can promote homeostasis and prevent mortality in aging flies. Interestingly, overexpression of MANF in neurons reduced lifespan (Supplementary Fig. 1c), suggesting that, in contrast to other cell types, elevated levels of MANF in neurons may have detrimental effects for organismal health, as recently suggested in mammals[30].

Mice with reduced MANF levels develop inflammation and liver damage

To test whether a role for MANF in aging would be conserved in vertebrates, we set out to assess inflammation in mice with MANF gain- and loss-of-function conditions.

Mice carrying a *Manf* null allele have been previously characterized[31]. In the C57BL/6 background, homozygosity for this allele is embryonic lethal[19], but animals kept in heterozygosity (MANFHet) survive with half the levels of MANF in circulation and in tissues (Fig. 3a and Supplementary Fig. 2a, see also[19]).

We evaluated the effects of reduced MANF levels on the development of inflammatory phenotypes. We found signs of sterile, chronic inflammation in the absence of other external stimuli: Increased infiltration and activation of macrophages (evaluated by F4/80 and CD68 staining) in white adipose tissue (WAT), liver and pancreas was detected at 5 months of age and was significantly higher in MANFHet mice at 10 months of age compared to WT littermates (Fig. 3b,c and Supplementary Fig. 2b,c). CD68 (Cluster of Differentiation 68) is a lysosomal membrane protein, expressed in macrophages, that is up-regulated by pro-inflammatory stimuli in actively phagocytic cells[32–35]. Such macrophage activation has also been associated with age-related chronic inflammatory diseases[36].

We also found signs of cellular senescence in MANFHet mice, but not WT littermates, at 10 months of age: elevated senescence-associated βGal activity in subcutaneous (Supplementary Fig. 2d) and visceral WAT (Fig. 3d), increased levels of 4-HNE adducts (Fig. 3e), and increased expression of p16 and IL-6 (Fig. 3f). In WT animals, senescent cells accumulate in old age, and are thought to contribute to the age-related loss of organismal homeostasis[2,37].

Aging is associated with alterations in tissue structure, function and cell composition, phenotypes that are accompanied by increased inflammation[1,2]. In the liver, for example, the apoptotic hepatocytes become more frequent, hepatic nuclear size and polyploidy increase, triglycerides accumulate, and liver fibrosis is observed[38–40] (see also Supplementary Fig. 3). The number of CD68+ macrophages (which are associated with liver damage and fibrosis[41]) also increases during liver aging[42] (Supplementary Fig. 3b-d). These observations are recapitulated in the livers of 10 months old MANFHet mice, with an increase in CD68+ macrophages, induction of cytokines and chemokines associated with tissue damage and pro-inflammatory activation (Fig. 3g), a decrease in the number of macrophages that express the anti-inflammatory marker Ym1[43] (Fig. 3h and Supplementary Fig. 2e), and increased levels of the pro-inflammatory cytokine IL-6 (Supplementary Fig. 2f). These observations indicate an acceleration of age-related pro-inflammatory states in MANFHet mice[44,45] (Supplementary Fig. 3e).

Transcriptome analysis comparing livers of 10 month old MANFHet mice and WT littermates confirmed the induction of genes associated with inflammation (CCL3, IL23, INFγ), and revealed induction of genes associated with apoptosis (Bcl2l14, casp4, Gadd45b) and collagen deposition (Col1a1, Col1a2, Col6a2, Col6a6, Col12a1) (Supplementary Fig. 2g-i; Supplementary Table 1), usually observed in association with liver damage[46]. We confirmed the induction of collagen and damage-associated genes by RT-qPCR (Supplementary Fig. 2j,p). Consistently, 10 month old MANFHet mice exhibited signs of liver damage: a significant increase in the number of phospho-JNK positive cells, in the levels of phospho-JNK in whole liver extracts (Fig. 3i and Supplementary Fig. 2k,l), increased numbers of γH2Ax-positive cells, increased hepatocyte apoptosis, and a significant increase in average hepatic nuclear size (Fig. 3j-m and Supplementary Fig. 2l). We further observed increased levels of collagen deposition in the liver and an expanded population of hepatic stellate cells (Fig. 3n and Supplementary Fig. 2m-o), indicative of liver fibrosis, and similar to what is observed in old animals[39,47] (Supplementary Fig. 3k-m).

The decline of MANF levels in aging mice, and the similarity of the phenotypes observed in the livers of middle aged MANFHet mice and old WT mice (Fig. 1b and Supplementary Fig. 3), support the notion that MANF loss contributes to age-related inflammation and liver damage.

Since liver damage, inflammation and fibrosis are also clinical manifestations in NASH patients, we asked whether this pathology was associated with a reduction in systemic MANF in humans. We evaluated the levels of MANF in serum samples from a cohort of NASH patients (53±18 years old) and age-matched healthy subjects (52± 16 years old) and found that human liver disease is associated with reduced levels of MANF in circulation (Fig. 3r).

Reduced MANF levels cause hepatosteatosis

Our transcriptome analysis of the livers of MANFHet mice also revealed alterations in several genes involved in lipid metabolism (Supplementary Fig. 2h), suggesting that MANF may also affect metabolic processes, as previously suggested in *Drosophila*[48]. We found, for example, that MANF induces G0/G1 Switch Gene 2 (G0S2), an important regulator of lipid

metabolism and inhibitor of lipolysis[49,50], suggesting a possible mechanism by which MANF loss may cause lipid accumulation in the liver. We confirmed its induction in the liver of 10 month old MANFHet mice (Supplementary Fig. 4a), as well as *in vitro* in human hepatocytes in which MANF was knocked down (HepG2, Supplementary Fig. 4b). Conversely, MANF overexpression in HepG2 cells resulted in repression of G0S2 (Supplementary Fig. 4c). These changes were not associated with changes in the canonical unfolded protein response (UPR) pathway, which has been associated with MANF function in other tissues[31](Supplementary Fig. 4a-c).

Livers from middle aged MANFHet mice indeed revealed structural changes indicative of the development of hepatosteatosis, supporting the idea that MANF deficiency is associated with lipid accumulation in hepatocytes (Fig. 3o-q and Supplementary Fig. 4d,e). The levels of triglycerides (TGs) in the liver of 10 month old MANFHet mice were significantly higher than in WT littermates of the same age, a difference that was not yet apparent in young (5 month old) animals of the same genotypes (Fig. 3p and Supplementary Fig. 4h,i). This suggests a progressive development of this disease state after a long period with reduced MANF levels.

Hepatosteatosis also develops progressively in animals under metabolic stress, as induced by a high-fat diet (HFD). Circulating levels of MANF showed a significant reduction in WT mice fed a HFD, approaching the levels observed in MANFHet animals (Supplementary Fig. 4f,g). MANF levels were not further changed, however, in young MANFHet animals fed a HFD (Supplementary Fig. 4g). Consistently, fat accumulation was similar in the livers of WT and MANFHet mice fed a HFD and the levels were identical to those found in middle aged MANFHet mice in the absence of metabolic stress (Supplementary Fig. 4h-j, see also Fig. 3p,q). Thus, the changes in MANF levels observed in WT animals under metabolic stress mimic those observed in MANFHet animals, both leading to progressive development of hepatic steatosis.

Unlike steatosis, the number of phospho-JNK positive cells and the total number and activation state of macrophages in the liver of young MANFHet animals were already higher than in WT littermates (Supplementary Fig. 4k-m), suggesting that a reduction in MANF levels causes early basal activation of macrophages and stress pathways. Importantly, these alterations were sufficient to increase hepatocyte susceptibility to apoptosis in response to signals imposed by metabolic stress: MANFHet mice at 5 months of age (a time point at which liver damage is not yet apparent under a normal diet) showed significant increase in hepatocyte apoptosis after exposure to a HFD, a phenotype of liver disease not observed in WT mice under similar metabolic stress (Supplementary Fig. 4n,o). However, livers of MANFHet mice did not show signs of liver fibrosis at this age (Supplementary Fig. 4p).

If reducing MANF levels is part of the mechanism by which a HFD produces the metabolic alterations leading to hepatosteatosis, then MANF delivery in mice fed a HFD should be protective and reduce fat accumulation in the liver. To test this hypothesis, we overexpressed MANF in young mice, prior to feeding a HFD (Fig. 4a). A stable systemic overexpression of MANF protein was achieved by hydrodynamic tail vein (HTV) injection of an enhanced episome vector (EEV) plasmid expressing hMANF. The stable expression of hMANF

(Supplementary Fig. 5a-d) during HFD feeding significantly reduced the accumulation of fat in the liver (Fig. 4b-d and Supplementary Fig. 5e), without affecting weight gain (Supplementary Fig. 5f). MANF overexpression also reduced the HFD-induced accumulation of activated (CD68+) macrophages in the liver (Fig. 4b,e). Maintaining high MANF levels during metabolic stress can thus indeed serve as a protective intervention against the development of hepatic steatosis and inflammation.

Immune cell-derived MANF and hepatocyte-derived MANF contribute to liver homeostasis

MANF is expressed in different cell types in the body and our previous work established that an autocrine function of macrophage-derived MANF is necessary for its tissue protective functions[19]. Thus, we sought to explore whether MANF derived from immune cells was also playing a role in the phenotypes observed in MANFHet mice. Cx3cr1 is a chemokine receptor expressed in a functionally distinct class of “resident” monocytes with immune patrolling activity and with a molecular profile of macrophage differentiation resembling alternative activation[51,52]. We used a tamoxifen-dependent Cx3cr1-driven Cre recombinase to conditionally ablate MANF in adult mice (Fig. 4f), and found that ablation of MANF in Cx3cr1- expressing cells is sufficient to recapitulate liver damage and inflammation observed in 10 month old MANFHet mice (Fig. 4g-m and Supplementary Fig. 5g-i). However, no change in liver fat content was observed after MANF ablation in immune cells (Supplementary Fig. 5j,k), suggesting that other cellular sources of MANF may contribute to maintain lipid homeostasis in the liver.

Since MANF is also expressed in hepatocytes, we sought to explore whether hepatocyte-derived MANF contributed to maintain liver homeostasis. To generate a mouse model in which MANF is specifically ablated in hepatocytes, we delivered an adeno-associated virus (AAV) coding for a Cre recombinase with hepatocyte-restricted expression (TBG-iCre) into mice carrying a $Manf^{fl}$ allele in homozygosity (Fig. 4n). This manipulation resulted in a liver-specific ablation of a portion of MANF genomic sequence and a consequent significant reduction in MANF levels in the liver (Supplementary Fig. 5l,m). Unlike what was observed after MANF ablation in immune cells, hepatocyte-specific ablation of MANF did not result in increased immune activation, liver damage or fibrosis (Fig. 4o-q and Supplementary Fig. 5n,o). Instead, these animals had increased levels of fat in hepatocytes (Fig. 4r,s and Supplementary Fig. 5p), a phenotype that was not present after MANF ablation in immune cells (Supplementary Fig. 5j,k).

Since systemic loss of MANF, as observed in MANFHet mice and old mice, results in hepatosteatosis and liver damage simultaneously, we propose that the effects observed when MANF declines systemically may be a consequence of the combined loss of MANF in different tissues. Interestingly, we did not detect any signs of senescence in the WAT of either mouse models at the tested age (data not shown).

MANF is necessary for liver rejuvenation by heterochronic parabiosis

Since MANF is found in circulation and its levels decline in old animals, we asked whether overall circulating levels of MANF affect tissue function, and whether restoring the levels of MANF in aged animals can improve tissue homeostasis.

First, we performed heterochronic parabiosis to test this idea. Parabiosis, the surgical joining of the circulatory system of two animals, allows the exchange of soluble molecules, thus providing a method to determine if specific circulating factors can alter tissue function. A large number of studies have established that heterochronic parabiosis, where animals of different ages are combined, results in the reversal of aging phenotypes in the old partner[3,5]. These studies have led to the widely-held model that young animals contain circulating factors that may be able to rejuvenate old tissues. Supporting this hypothesis, recent studies have shown that rejuvenation of regenerating compartments in the brain, as well as of liver structure, can be achieved by merely injecting plasma from young animals[3,6,53].

To ask whether MANF contributes to the rejuvenating effects of heterochronic parabiosis, we generated heterochronic pairs in which 20 month old WT mice were combined with either 4 month old MANFHet (O-YgHet) or WT (O-YgWT) littermates, and maintained for 5 weeks before analysis (Fig. 5a). We reasoned that if MANF is one of the factors mediating the rejuvenating effect by the young partner, then these effects should be attenuated in old animals from O-YgHet pairs. We focused on age-specific alterations in the liver which have been well described[39,40] and validated in this study (Supplementary Fig. 3).

Consistent with previous reports describing liver rejuvenation by heterochronic blood exchange[6], the accumulation of fibrotic areas in old livers was significantly reduced in O-YgWT pairs and was accompanied by a reduction in hepatic stellate cell numbers (Fig. 5b,c and Supplementary Fig. 6a-c). Moreover, we found that heterochronic parabiosis further reversed other hallmarks of liver aging: Livers of old mice exposed to a young WT circulatory system had significantly less phospho-JNK positive cells and γH2Ax-positive cells and a significantly lower number of apoptotic hepatocytes (Fig. 5d-g and Supplementary Fig. 6b) than O-O animals. The CD68+ cell population was also significantly reduced in old livers from O-YgWT pairs when compared with O-O livers, while no changes were found in the total number of F4/80+ cells in isochronic and heterochronic pairs (Fig. 5h and Supplementary Fig. 6b,d), as expected for a parameter unaffected by aging (Supplementary Fig. 3c, see also[39,42]). We did, however, observe a significant reduction in IL-6 transcripts in old livers after exposure to young partners (Fig. 5i). Exposure to a young circulatory environment is, thus, sufficient to reverse phenotypes of age-related liver damage and inflammation.

Strikingly, in old animals exposed to a young MANFHet circulatory system, these rejuvenating effects of heterochronic parabiosis were significantly impaired (Fig. 5b-i and Supplementary Fig. 6a-c), suggesting that MANF is one of the beneficial factors present in young blood.

Average hepatocyte nuclear size and hepatosteatosis were two age-related phenotypes (Supplementary Fig. 3) that were not reversed by exposure to a young wild-type circulatory environment (Supplementary Fig. 6e-g). Thus, we could not evaluate the requirement of MANF to reverse these phenotypes.

To gain further insight into the contribution of MANF to the rejuvenating effects induced by heterochronic parabiosis, we performed RNA sequencing on liver samples from the different

experimental groups (Fig. 5j,k and Supplementary Fig. 6h,i; Supplementary Table 1). We found 1022 genes significantly induced and 306 genes significantly repressed in the liver of old mice. Supporting the existence of a rejuvenating effect by heterochronic parabiosis, 19% of the genes induced by aging (199 genes) and 41% of the genes repressed by aging (126 genes) were significantly restored to young levels in the old animal exposed to the young circulatory environment. Interestingly, among all these genes (325), 63% were dependent on MANF, as they did not show significant changes in old livers from O-O pairs when compared to old livers from O-YgHet pairs. These included 77% of the repressed genes and 55% of the induced genes. KEGG (Kyoto Encyclopedia of Genes and Genomes) pathway analysis of the set of genes changed by heterochronic parabiosis in a MANF dependent manner showed enrichment for circadian rhythm and metabolic pathways, the same set of pathways found enriched in the set of all restored genes (Fig. 5k and Supplementary Fig. 6i). These data are in line with recent reports supporting an important contribution of deregulated circadian rhythms to liver aging[54], and consistent with our observations supporting a function of MANF in metabolic pathways (Supplementary Fig. 2 and 4) and its requirement for the full rejuvenating effects of heterochronic parabiosis in the liver (Fig. 5 and Supplementary Fig. 6).

MANF delivery ameliorates liver damage, inflammation and metabolic dysfunction in old mice

This beneficial function of MANF in liver homeostasis prompted us to test whether restoring youthful expression of MANF in aged mice directly could reverse hallmarks of liver aging. Young and old mice received hMANF HTV injections and were analyzed 5 weeks post intervention (Fig. 6a). Consistent with its described immune modulatory properties[19], hMANF overexpression (Supplementary Fig. 7a,b) resulted in a significant reduction of activated macrophages (Fig. 6b and Supplementary Fig. 7c) in the liver, while the total number of macrophages, evaluated by F4/80 expression, was not altered (Supplementary Fig. 7d). The protein levels of the pro-inflammatory cytokines IL-6 and IFNγ were also significantly reduced in the liver of old animals that received injections of MANF plasmid (Fig. 6c,d). Furthermore, age-associated signs of liver damage, and hepatocyte apoptosis (Fig. 6e,f and Supplementary Fig. 7e,f) were significantly reduced after hMANF expression, resembling the liver rejuvenation elicited by heterochronic parabiosis (Fig. 5). Liver fibrosis, however, was only partially rescued, as we observed a significant reduction in hepatic stellate cell numbers, but not a full reversion in collagen deposition (Supplementary Fig. 7e,g,h). Since MANF overexpression was sufficient to reverse markers of inflammation, liver damage and apoptosis, it is possible that this intervention may prevent further development of fibrosis, but may not be sufficient to reverse the collagen deposition that has already occurred. Since liver fibrosis is rescued by heterochronic parabiosis in a MANF-dependent manner (Fig. 5b,c and Supplementary Fig. 6a-c), it is likely that additional circulatory factors are cooperating with MANF to resolve already existing fibrosis.

Overexpression of MANF by HTV injection results in increased levels of MANF in the liver but also in circulation (Supplementary Fig. 5a-d and Supplementary Fig. 7a,b). Thus, the effects observed could be due to increasing MANF levels in circulation, in the liver or a combination of both. To test whether increasing circulating levels of MANF is sufficient to

elicit the same effects, we treated old mice with intra peritoneal (i.p.) injections of human recombinant MANF (hrMANF) protein (Fig. 6g and Supplementary Fig. 8a). This treatment was sufficient to improve several hallmarks of liver aging: We observed reduction in markers of inflammation, cellular damage, hepatocyte apoptosis, and hepatic stellate cell numbers, but not a complete resolution of existing fibrosis (Fig. 6h-l and Supplementary Fig. 8b-f). Increasing the circulating levels of MANF is thus sufficient to elicit the same effects as MANF overexpression by HTV injection, suggesting that, at least in part, the effects observed are due to MANF acting as a secreted factor.

Interestingly, although age-associated inflammation and liver damage could be ameliorated by both methods of MANF supplementation, the accumulation of TGs in the liver of old mice was not reversed (Supplementary Fig. 7i,j and Supplementary Fig. 8g,h). These data suggest that while some liver aging phenotypes can be dynamically reversed or improved with interventions at old age, other aging phenotypes, such as hepatosteatosis, which develops over long periods of time, may require a preventive approach (See Fig. 4a-d and Supplementary Fig. 5e).

To gain further insight into the beneficial effects of MANF in the old liver, we performed RNAseq analysis in livers after MANF overexpression by HTV injection. Of 887 genes significantly affected by aging in the liver in these experiments, 12% were restored by MANF overexpression (Supplementary Fig. 9a; Supplementary Table 1). This included genes involved in lipid metabolic processes and signal transduction (Supplementary Fig. 9b-d). Importantly, we observed a significant repression of age-induced G0S2 transcripts in the liver (Supplementary Fig. 9b,d), a transcriptional effect also observed in the liver of animals subjected to rejuvenating interventions[55,56].

Moreover, increasing MANF levels in old mice led to a significant improvement in glucose tolerance (Fig. 6m), a parameter which declines in old mice[57], insulin tolerance (Fig. 6n), and a partial restoration of fasting glucose levels, while maintaining their body weight (Supplementary Fig. 9e-h). These observations suggest that the effects of MANF treatment extend beyond the liver and may contribute to an improvement in general metabolic health.

Together, our data support the idea that MANF supplementation could be explored as an effective intervention to allay age-related metabolic and inflammatory dysfunctions, and to prevent the development of hepatic steatosis induced by metabolic stress.

Discussion

Our work identifies a novel function for MANF in maintaining metabolic and immune homeostasis. The age-related decline in MANF expression in flies, mice and humans, the loss of intestinal homeostasis in MANF deficient flies, the loss of immune and metabolic homeostasis in MANF deficient mice, and the loss of the rejuvenating effects of heterochronic parabiosis when performed with MANF heterozygotes, indicate that the age-related loss of MANF contributes to the decline of tissue and metabolic function (Fig. 6o). The fact that MANF supplementation is sufficient to extend lifespan in flies, and to improve

several hallmarks of liver aging and age-related metabolic dysfunction, indicates a potential therapeutic application for MANF in age-related diseases.

The importance of systemic factors in the aging process has been repeatedly demonstrated in heterochronic parabiosis studies[3,5,6]. The identification of such systemic factors is critical for the development of effective rejuvenating interventions. Our results define a subset of MANF-dependent liver phenotypes that are rejuvenated during parabiosis and are also reversed by systemic delivery of MANF, supporting the notion that MANF is indeed one of the circulating factors responsible for the rejuvenating effects of heterochronic parabiosis. Interestingly, although MANF delivery was sufficient to reduce the age-related increase in damage and hepatic stellate cell numbers, it was not sufficient to fully resolve fibrosis, suggesting that other circulating factors contribute to the rejuvenating effects elicited by young plasma. Oxytocin, tissue inhibitor of metalloproteinase 2 (TIMP2), growth differentiation factor 11 (GDF-11) and gonadotropin-releasing hormone (GnRH)[53,58–60] are examples of other circulating factors shown to have systemic rejuvenating properties and may contribute to this effect. Interestingly, among the beneficial factors identified so far, MANF is the only one with described immune modulatory properties[19], and is thus particularly interesting in the context of aging[61]. Future work will be required to investigate whether the beneficial effects of MANF extend beyond the liver and whether regulation of inflammation is indeed part of the mechanism through which rejuvenation is promoted.

The established anti-inflammatory effect of MANF may not be the only beneficial property of MANF. Our analysis of the liver transcriptome after heterochronic parabiosis revealed an important contribution of metabolic pathways to the MANF-dependent effects on liver homeostasis. The ability of MANF to regulate metabolic pathways was previously suggested in *Drosophila*[48] and complete loss of MANF in another metabolic organ, the pancreas, leads to severe type-1 diabetes due to loss of β-cell mass[31]. In this context, the effects were mediated through chronic UPR activation which compromised cell viability[31]. Although chronic UPR activation has been associated with liver disease[62], we did not observe changes in canonical UPR components in the liver of mice with reduced MANF levels, or in hepatocytes where MANF was knocked down. Furthermore, β-cell viability was not compromised in our MANFHet animals since they had normal glucose tolerance profiles and pancreas histology revealed no abnormalities in tissue morphology. Instead, we found that several genes involved in lipid metabolism were up-regulated in the liver of MANFHet mice. Among those, G0S2 was one of the genes showing the most consistent regulation by MANF, being induced by MANF knock down and repressed by MANF delivery *in vivo* and *in vitro*. Increased levels of G0S2 in the liver promote hepatic steatosis, while G0S2 deletion can prevent hepatic triglyceride accumulation, in agreement with what we observe in mice with reduced MANF levels[63–65]. Interestingly, regulation of G0S2 by MANF is also observed in macrophages (our unpublished data) and G0S2 up-regulation is associated with pro-inflammatory states[66]. G0S2 may thus constitute a target of a common molecular pathway regulated by MANF in different biological contexts. It will be interesting to investigate whether G0S2 is part of the mechanism through which MANF mediates its lipid metabolic functions.

With respect to age-related liver disease in particular, there is evidence for a synergistic effect between chronic activation of stress signaling, metabolic deregulation, and increased inflammation[67]. Aging is believed to promote liver disease by increasing both inflammation and susceptibility to liver damage[68], and anti-inflammatory interventions can alleviate several hallmarks of liver aging[16]. Our experiments involving conditional ablation of MANF in different cell types support the notion that reducing MANF levels in different tissues contributes to different aspects of liver disease. Thus, in animal models where systemic levels of MANF are reduced (old mice and MANFHet mice), it is likely that liver disease is the result of the combinatorial loss of MANF in different tissues. Because the levels of MANF are decreased systemically in NASH patients, and in elderly individuals, it is possible that, also in humans, liver disease results from similar interactions of MANF signaling in different cell types. Interestingly, it was recently reported that in newly diagnosed prediabetic and diabetic patients circulating levels of MANF are increased[22]. Since MANF is a stress responsive protein, induced in several damage conditions where it has a protective effect[24], it is possible that these findings reflect a case where MANF loss is not at the cause of the disease, but constitutes an early protective stress response to a pathogenic state. Conversely, a genetic mutation in MANF has been associated with type-2 diabetes in a 22-year-old young woman[69]. Interestingly, this mutation was also associated with other pathologies, including hypothyroidism, obesity, deafness, high myopia, microcephaly and partial alopecia[69]. Thus, it is likely that loss of MANF is associated with age-related pathologies beyond liver disease. Consistently, our ongoing research indicates that skeletal muscle mass, a parameter that is reduced in old animals[70], may be another age-related phenotype affected by MANF (Supplementary Figure 10).

We observe that phenotypes developed in middle aged MANFHet mice or after HFD feeding are not acute responses to MANF loss, but happen several months after MANF levels decline. Also during physiological aging, MANF levels decline gradually but disease phenotypes only manifest at old age. Our interpretation is that a reduction in systemic MANF levels renders the organism susceptible to stress stimuli, and that this results in disease states when the animal is exposed to metabolic stress. During normal aging, as stress is experienced, MANF deficiency will thus lead to an acceleration of the onset and progression of pathologies that normally occur over the course of the animal's lifespan. We propose that MANF and its signal transduction pathway(s) constitute promising new targets for intervention into aging and age-related diseases.

Methods

Animals

Mice—All mice used in the described studies, other than parabiosis studies, were housed and bred at the AAALAC accredited vivarium of The Buck Institute for Research on Aging in a Specific Pathogen Free (SPF) facility and housed in individually ventilated cages on a standard 12:12 light cycle. All procedures, other than parabiosis, were approved by the Buck Institute Institutional Animal Care and Use Committee (IACUC).

Mice used in the parabiosis studies were housed under SPF conditions on a standard 12:12 light cycle and experiments were performed in accordance with institutional guidelines approved by the University of California San Francisco IACUC.

All studies were done in C57BL/6JN male mice. Old WT mice used for tissue analysis, HTV injections, hrMANF injections and parabiosis experiments and young WT mice used for HTV experiments were obtained from the National Institute of Aging. Young WT mice used in HTV experiments combined with HFD and all sets of littermates containing WT and MANFHet mice used in parabiosis and all other studies were bred in house.

Manf heterozygous mice were obtained from UC Davis KOMP Repository Knockout mouse project (clone MANF_D06 (EPD0162_3_D06; C57Bl/6N-Manftm1a(KOMP)Wtsi). These mice carry a b-galactosidase reporter cassette with a strong splice acceptor site inserted in the intron between exon 2 and exon 3 of the Manf gene, creating a constitutive null mutation through splicing of exon 2 to the reporter cassette. Mice carrying this null allele have been previously characterized[31]. Mice obtained from the UC Davis KOMP repository were generated in a C57Bl/6N background and backcrossed into C57Bl/6J in our facility. Primers used for genotyping for the Manf allele (wt vs. null) are listed in Supplementary Table 2.

Mice carrying and $Manf^{fl}$ allele were generated in house by crossing mice carrying the MANF disruption cassette with a mice carrying a constitutive transgene coding for the flipase protein (Rosa26::Flpo, JAX stock nr.. 012930). Flipase mediated excision of the disruption cassette reconstitute a functional Manf gene in which exon 3 is flanked by loxP sequences. Primers used for genotyping for the $Manf^{fl}$ allele are listed in Supplementary Table 2.

To generate mice with conditional ablation of Manf in Cx3cr1 expressing cells we generated $Manf^{fl/fl}$, $Cx3cr1^{CRE\text{-}ER/+}$ mice. Mice carrying the $Cx3cr1^{CRE\text{-}ER}$ allele are B6.129P2(Cg)-Cx3Cr1tm2.1(CRE/ERT)Litt/WganJ and were purchased from The Jackson Laboratory (JAX, stock nr. 021160). In these mice, a CreER-IRES-EYFP cassette replaces the first 390 bp of the second Cx3cr1 exon[71]. Heterozigous carriers of the allele were used on the study. Primers used for genotyping for the Cx3Cr1 allele (wt vs null) are listed in Supplementary Table 2. To induce Cre activity 2 month old mice received daily i.p. injections of tamoxifen (75mg/Kg mouse, Sigma) for 5 consecutive days and were analyzed 3 months after tamoxifen treatment. Control mice were littermates of the same genotype that received sham injections (corn oil, Sigma) or $Manf^{fl/fl}$ mice without the $Cx3cr1^{CRE}$ allele / $Cx3cr1^{CRE/+}$ mice without the $Manf^{fl}$ allele, that received tamoxifen injections.

Drosophila stocks—Flies were cultured on yeast/molasses-based standard fly food (recipe: 10L H2O, 138g agar, 220g molasses, 750g malt extract, 180 dry yeast, 800g corn flour, 100g soy flour, 62.5ml propionic acid, 20g Methyl 4-Hydroxybenzoate, and 72ml ethanol). For GeneSwitch experiments, 86 mg RU486 was additionally dissolved in the ethanol for 200 μM final concentration. Flies were maintained at 25°C with a 12h light/dark cycle and 65% humidity. All flies used in the experiments reported were females.

Fly lines HmlΔ::Gal4, LSP2::Gal4, Elav::Gal4 and W^{1118} were provided by the Bloomington Drosophila Stock Center. RNAi line MANFRNAiv12834 (UAS::MANFRNAi) was obtained from the Vienna Drosophila RNAi Center. These construct has no predicted off-targets. MANFRNAiv12834 was combined with a transgene driving Dicer overexpression (UAS::DICER2) to achieve efficient MANF knock-down[19].

We received the following lines as gifts: UAS::MANF, (T. Heino); NP1::Gal4 (D. Ferrandon); PPL::Gal4 (M. Pankratz); Upd3::Gal4 (N. Perrimon); C7::Gal4 (M. Uhlivora); UAS::Upd2 (M. Zeidler); UAS::Upd3 (N. Buchon); 2xStat::GFP (E. Bach).

Fly aging and demographics

Progenies ware collected 3 days after the first fly hatched and flies were allowed to mate for 2–3 days. Female flies of the indicated genotypes were then separated into vials at a density of 40 flies or less flies per vial and aged at 25°C.

For aging and lifespan experiments fly food was changed three times a week. For lifespan experiments death events were recorded visually at the day of food change. For lifespan experiments fly densities were as follow: Act5c::GS>MANFRNAi (23–34 flies/vial, Fig. 2a); HmlΔ::Gal4>MANFRNAi (12–18 flies/vial, Fig. 2c); PPL::Gal4>UAS::MANF (25–30 flies/vial, Fig. 2h); LSP2::Gal4>UAS::MANF (16–32 flies/vial, Fig. 2h); HmlΔ::Gal4>UAS::MANF (27–37 flies/vial, Fig. 2i); Upd3::Gal4>UAS::MANF (17–28 flies/vial, Fig. 2j); Elav::Gal4>UAS::MANF (24–32 flies/vial, Supplementary Fig. 1c);

In vivo procedures in mice

Diets—For studies involving feeding a HFD, Rodent diet with 60% kcal%fat (D12492, Research diets) was used as HFD and Rodent diet with 10% kcal% fat (D12450, Research diets) was used as control diet. For all other studies animals were kept on a normal chow diet: Pico Labs 20% protein diet (formula 5058) for animals on the parabiosis studies and Teklad Global 18% Protein Rodent diet (2018, Harlan) for all other studies and animals analyzed at different ages. “Cntrl” refers either to the control diet or normal chow diet.

Parabiosis—Parabiosis surgery followed previously described procedures[3,72]. Briefly, mirror-image incisions at the left and right flanks were made through the skin and shorter incisions were made through the abdominal wall. The peritoneal openings of the adjacent parabionts were sutured together. Elbow and knee joints from each parabiont were sutured together and the skin of each mouse was stapled (9mm Autoclip, Clay Adams) to the skin of the adjacent parabiont. Each mouse was injected subcutaneously with the antibiotic Enrofloxacin (5mg/Kg), anti-inflammatory Carprofen (5mg/Kg) and the analgesic buprenorephrine (0.1mg/Kg) as directed for pain and monitored during recovery. For overall health and maintenance behavior, several recovery characteristics were analyzed at various times after surgery, including paired weights and grooming behavior.

AAV injections—For conditional ablation of MANF in hepatocytes we delivered 2.5×10^{11} gc of AAV8-TBG-iCre[73] (VB1724, Vector Biolabs, lot 180409#24) or AAV8-TBG-eGFP (VB1743, Vector Biolabs, lot 180312–180420) in 100μl of saline solution (0.9% sodium

Chloride injection, USP, RL-4492, Hospira), through a tail vein injection in 6–7 month old $Manf^{fl/fl}$ mice. Animals were analysed 6 weeks after AAV delivery and liver-specific genomic ablation was confirmed by PCR (Supplementary Fig.5l).

HTV injections—For hMANF overexpression by hydrodynamic tail vein injection, 2 μg of plasmid coding hMANF (EEV604A-2-CAGs-hManf, CS950EEV-1, Systems Biosciences) or control plasmid (EEV604A-2-CAGs-gfp-Luc, CS950EEV-1, Systems Biosciences) were injected as described[74]. Briefly, animals were weighed and 10% of body weight in grams was determined. Injections were prepared for each mouse, containing 2 μg of plasmid diluted in a volume of saline solution equivalent to 10% of animal body weight in ml. Animals were anesthetized and the full volume of injection was delivered through the tail vein within 10 seconds. Animals were allowed to recover and monitored carefully after the procedures. Animal weights were recorded weekly during the study. At the end of the study, levels of hMANF in the liver were evaluated by RT-qPCR, Western blot and immunostaining and only animals where MANF overexpression could be detected by at least 2 of the methods were included in the study.

i.p injections of hrMANF—21 month old C57Bl/6JN mice received 0.7mg hrMANF protein (P-101–100, Icosagene, batch 030513) per Kg of body weight through intraperitoneal injections in saline solution, three times per week during 5 weeks. Animal weights were recorded weekly during the study. Human MANF protein was detected in blood samples from these animals confirming the systemic delivery.

Glucose tolerance test and Insulin tolerance test—Glucose and insulin tolerance tests were performed on mice that were fasted for 4 hours. Insulin (0.75 U/kg) or glucose (2 g/kg) were intraperitoneally injected into mice and glucose concentrations were determined with an Accu-Chek Advantage glucometer (Roche) in blood collected from the tail vein at the indicated time points.

HepG2 cell culture

HepG2 cells (ATCC, HB-8065) were cultured in DMEM supplemented with 10% FBS. For MANF silencing, 200,000 HepG2 cells were transfected with 10μl of a 5μM solution of either ON-TARGETplus SMARTpool human Manf siRNA (L-012158–00, Dharmacon) or ON-TARGETplus Non-targeting Pool (D-001810–10, Dharmacon), using Stemfect™ RNA transfection reagent (Stemgent, 02–0005), according to manufacturer's instructions. Media was changed 24h after transfection and cells were collected 48h after transfection.

For MANF overexpression experiments, cells were infected with lentivirus produced from plenti6.3 eGFP-hMANF (Gift from M. Henderson and B. Harvey, NIH/NIDA, Baltimore, MD, USA) or EF1α-GFP (Gift from Dr. Charles Murry, UW, Seattle). Lentiviral generation was performed as reported[75]. Briefly, the viruses were generated by co-transfection of the vector and the packaging constructs (VSVg, Gag/Pol, Rev) in the 293T cell line by the calcium phosphate precipitation technique. The following day, the precipitates were removed and fresh medium was added. This medium, containing the viral particles, was recovered 48h later and centrifuged at 3,000 x g for 10 min. 200,000 HepG2 cells were

infected media containing the viral particles supplemented with polybrene (Sigma). Media was changed 24h later, and cells were cultured in DMEM containing 10% FBS for additional 24h before collection.

Histological analysis, Imaging and Quantification methods

Mouse tissue harvesting and storage—Animals were euthanized and blood was collected by heart puncture in EDTA-coated tubes for plasma preparation. Animals were perfused with PBS and tissues were harvested and split into samples.

Samples processed for histology were fixed over-night at 4°C in 4% Paraformaldehyde in PBS (4%PFA). Fixed tissues processed for cryopreservation were washed with PBS and incubated with 30% sucrose in PBS overnight at 4°C. Sucrose treated tissue was embedded in OCT in cryomolds (Tissuetek) and frozen on dry ice. Skeletal muscle was directly embedded in OCT in cryomolds (Tissuetek) without fixation and frozen in Methyl-butane submerged in liquid nitrogen. Frozen embedded tissue was cryosectioned at 10um thickness, collected on Superfrost Plus microslides (VWR) and stored at 80°C until analysis. Fixed tissues processed for paraffin embedding were washed with PBS, serially dehydrated in 30%, 50%, and 70% ethanol at RT and processed in a Leica TP 1020 benchtop tissue processor in Monosette IV Cassettes (VWR), using the following protocol: 44 min incubations in serial 70%, 80%, and 90% ethanol, 2× 30 min incubations in 95% ethanol, 2× 1 hour incubations in 100% ethanol, 2× 22 min incubations in xylene and 2× 2 hour incubations in Paraplast Plus (VWR) under vacuum. Tissues were embedded in Paraplast Plus at 60°C in a HistoCore Arcadia Embedding System (Leica) and sectioned on a RM 2255 microtome (Leica) at 7μm thickness, collected on Superfrost Plus microslides (VWR) and stored at room temperature until analysis.

Samples processed for RNA, protein and lipid isolation were flash frozen in cryotubes submerged in liquid nitrogen.

Immunostaining of mouse cryosections and nuclei staining—Cryosections collected on slides were thawed, permeabilized with PBS containing 0.1% Tween20 (PBT) for 15 min at RT, blocked with 10% donkey serum (Jackson ImmunoResearch) in PBT and incubated with primary antibody, diluted in blocking solution, overnight at 4°C. Primary antibody was washed 3x with PBT and detected using Alexa conjugated secondary antibodies (Invitrogen, Molecular Probes). Secondary antibody was washed 6x with PBT. Nuclei were stained for 5min with 300nM DAPI (4',6-diamidino-2-phenylindole) in PBS at RT. Neutral lipids were stained for 5 min with 50μg/ml Bodipy 493/503 (Invitrogen, D3922) in PBS at RT. Slides were rinsed in PBS and mounted with Fluoromount G media (17984–25, Electron Microscopy Sciences) and micro cover glass No. 2 (48382–128, VWR). Staining of pJNK, γh2Ax and cCasp3 included an additional step of permeabilization involving 2 min incubation in boiling 10mM Citrate buffer. For information on primary antibodies used see Supplementary Table 3.

TUNEL staining of mouse cryosections—Cryosections collected on slides were thawed and hydrated in PBS for 15 minutes at RT. Tissue was permeabilized for 2 min in boiling 10mM Citrate buffer and washed 3 times with PBS while cooling down to RT.

Cryosections were incubated in the dark for 1h at 37°C with 50μl of TUNEL reaction mixture (In situ cell death detection kit, TMR Red, Roche) prepared according to manufacturer's instructions. Slides were rinsed three times with PBS, counterstained with DAPI and mounted as described above.

OilRedO staining of mouse cryosections—Cryosections collected on slides were thawed, fixed in 4% PFA for 20min and hydrated in PBS for 10 min at RT. For OilRedO staining cryosections were rinsed in 60% isopropanol for 5 min, stained with freshly prepared 0.5% Oil Red (Sigma) in isopropanol, diluted 3:2 in distilled water, for 20 min at RT. Slides were washed in 60% isopropanol for 5 min, rinsed in distilled water and mounted with 80% tris-buffered glycerol.

Sirius Red staining of mouse cryosections—Cryosections collected on slides were thawed and fixed in 56C Bouin's Solution for 1 hour, rinsed twice in distilled water and stained in Picrosirius Red Solution (Polysciences) for 1 hour, washed in 0.1N hydrochloride Acid (Polysciences) for 5min, serially dehydrated in 90%, 95%, and 100% ethanol, washed twice in xylene for 2 min and mounted with Permount Mounting Meduim (Electron Microscopy Sciences).

Hematoxylin and Eosin staining of mouse sections—Sections from paraffin embedded livers or muscle cryosections collected on slides were stained with Modified Mayer's Hematoxylin (Sigma) for 2 min, and with Eosin Y (Sigma) for 1 min. Muscle cryosections were fixed in cold 4% PFA for 20 min on ice prior to H&E staining. Between stains tissue was washed as follows: 2x rinse in distilled water, 10% acetic acid for 1 min, 2x rinse in distilled water, Scotts Tap Water for 2 min, rinse in distilled water and 70% ethanol for 1 min. Stained tissue was rinsed in 90% ethanol, serially dehydrated in 90%, 95%, and 100% ethanol, incubated twice in xylene for 2 min and mounted with Permount Mounting Medium (Electron Microscopy Sciences). Sections from paraffin embedded livers were serially deparaffinized before staining.

pH3 staining of Drosophila guts—Adult female *Drosophila* guts were dissected in PBS, fixed for 45min at room temperature in fixative (100 mM glutamic acid, 25 mM KCl, 20 mM MgSO4, 4 mM sodium phosphate, 1 mM MgCl2, and 4% formaldehyde), washed for 1 h at 4°C in washing buffer (1x PBS, 0.5% bovine serum albumin and 0.1% Triton X-100), and then incubated in primary antibody recognizing phospho histone H3 (4°C overnight) and secondary antibodies (4°C for 4 h or overnight) in washing buffer, between which was 1 h washing at 4°C. DAPI was used to stain DNA. For information on primary antibodies used see Supplementary Table 3. The number of pH3 positive cells/midgut was counted by direct observation under the microscope.

Imaging—All preparations were imaged using a Zeiss LSM 700 confocal laser scanning microscope.

Quantifications in mouse Liver and muscle sections—For all quantifications, 4–8 random 1024×1024px fields from confocal captures of liver sections from each animal were used. Cell numbers were counted using the appropriate channels in combination with DAPI

to identify nuclei, using the analysis count tool in Photoshop CS3 extended. Nuclear area was calculated in DAPI stained sections in arbitrary units (a.u.), using ImageJ software after scale normalization (Rasband, W.S., ImageJ, U. S. National Institutes of Health, Bethesda, Maryland, USA, http://imagej.nih.gov/ij/, 1997–2014.). For each random field of each animal 100–200 nuclei were counted. Bodipy and Desmin were quantified as the %area occupied by the signal in the corresponding channel using a standardized threshold for all images on ImageJ. OilRedO and Sirius Red were quantified as the %area occupied by the red signal. Red signal was segregated from a bright field image captures by isolating the green channel and quantified using a standardized threshold for all images on ImageJ. For all parameters, counts from all fields corresponding to one animal were averaged and represented as one dot in the graphs. In all graphs one dot represents one animal. Skeletal muscle cross-sectional area was quantified using ImageJ after scale normalization.

Steatosis evaluation in liver sections—Dr. Huifei Liu evaluated steatosis in liver sections stained with Hematoxylin and Eosin (H&E) and OilRedO. Steatosis was scored based on H&E stainings according to observed levels of macrovesicular steatosis typically distributed around zone 3, around the central veins. Scores were attributed based on the percentage of hepatocytes involved in the phenotype, as follows: 0, <5%; 1, mild: 5–33% hepatocytes involved; 2, moderate: 34–66% hepatocytes involved; 3, marked:>67% hepatocytes involved. In addition, signs of microsteatosis, not considered for steatosis scoring, were evaluated based on OilRedO staining.

Mouse plasma analysis

Blood was collected from animals fasted for 4h using the submandibular pouch technique (or heart puncture if animals were euthanized for tissue collection) in EDTA-coated tubes. Blood was centrifuged for 15 minutes at 2,000g and the plasma supernatant was recovered and stored at −80°C until analysis. MANF concentrations in mouse plasma were determined with MyBiosource mouse MANF ELISA kit (MyBiosource, MBS2025592) in plasma samples diluted 1:1 in PBS supplemented with protease inhibitors (Sigma), according to manufacturer's instructions. Recombinant MANF protein concentrations in mouse plasma (HTV experiments and i.p. injection experiments) were determined with Icosagen human MANF ELISA kit (Icosagen, K2–004-096) in plasma samples diluted 1:1 in PBS supplemented with protease inhibitors (Sigma), according to manufacturer's instructions.

Human serum analysis

Human serum samples were obtained commercially from BioreclamationIVT. All samples of human serum were recovered from whole blood donations of male subjects, according to the commercial source. Human MANF concentrations in human serum were determined with Cloud-clone corp. human MANF ELISA kit (Cloud-clone corp., SEC300Hu) in serum samples diluted 1:10 in PBS supplemented with protease inhibitors (Sigma), according to manufacturer's instructions.

Triglyceride quantification

Liver samples were homogenized in 50 μL extraction buffer (5 vol isopropanol, 2 vol water, 2 vol Triton X-100), per mg of tissue and supernatant lipid extracts were recovered by

centrifugation. Triglyceride quantification was performed in undiluted samples using Stanbio Triglyceride Liquicolor (Stanbio, 2100–430), according to manufacturer's instructions.

Hydroxyproline quantification

Liver samples were homogenized in 100 μL of distilled water per 10 mg of tissue. 100 μL of the homogenate was mixed with 100 μL of 12N hydrochloric acid and samples were hydrolyzed for 3h at 120ºC in Teflon caped pressure tight vials. Supernatant was cleaned of cellular debris with 5mg of activated charcoal and recovered by centrifugation. Hydroxyproline (HP) content of each sample was determined using Cell Biolabs HP assay kit (Cell Biolabs, Inc., STA-675), according to manufacturer's instructions.

Reverse-Transcription and Real-Time quantitative PCR (RT-qPCR)

Total RNA from frozen liver samples, frozen WAT samples, freshly dissected *Drosophila* midguts (8/sample) or HepG2 cells was extracted using TRIzol and cDNA was synthesized using 500–1000ng of RNA and iScript cDNA synthesis kit (BioRad). Real-time PCR was performed on a Bio-Rad CFX96™ detection system, using SsoAdvanced™ Universal SYBR® Green Supermix (BioRad). Quantification of expression for each gene in each sample was normalized to GAPDH (human samples, HepG2), beta-actin (mouse samples) or Actin5c (fly samples) and results are shown as gene expression levels relative to levels in control samples which are arbitrarily set to one. For information on primer sequences see Supplementary Table 4.

RNA sequencing and bioinformatic analysis

RNA prepared as described above was used as template to generate RNASeq libraries for Illumina sequencing (TruSeq Stranded mRNA LT Kit). Libraries were sequenced using an Illumine HiSeq 4000. Between 27,470,320 and 34,586,527 Million 150bp PE reads were generated for the samples of the parabiosis experiment, between 60,706,154 and 80,734,144 reads were generated for the MANFHet experiment, and between 19,686,618 and 29,894,103 reads per sample were generated for the HTV experiment. Reads were mapped to the Mouse genome Release mm10 using STAR (v2.4.2a). Gene expression level was quantified with HTSeq using GENCODE annotation M10, recorded as RPKM (Reads Per Kilobase of transcript per Million mapped reads) and further analyzed using Excel. GO and KEGG analysis was carried out using The Database for Annotation, Visualization and Integrated Discovery (DAVID, https://david.ncifcrf.gov/,[76]).

Western Blots

Liver samples, WAT samples, skin samples and muscle samples or whole *Drosophila* (5/sample) were homogenized in IP buffer supplemented with protease inhibitors (Sigma) and phosphatase inhibitors (Sigma) for 45 min at 4°C and supernatant protein extracts were recovered by centrifugation. Protein concentration in samples was determined using Protein coomassie assay reagent (ThemoScientific).

Western blot analyses were performed on 10%−15% SDS-PAGE. After electrophoretic transfer of proteins from SDS-PAGE gels to nitrocellulose membranes using a Trans Blot

Turbo Transfer system (BioRad), the membranes were blocked with Tris-buffered saline-0.1% Tween 20 containing 5% milk for 1h and incubated overnight at 4°C with primary antibodies. Membranes were then washed and incubated 1h with a peroxidase-conjugated secondary antibody (1:5000; BioRad), and developed using the Pierce ECL western blotting substrate (ThemoScientific, 32209). For information on primary antibodies used see Supplementary Table 5.

IL-6 ELISA and IFNγ in liver extracts

IL-6 quantification was performed in undiluted protein samples (prepared as for western blot analysis) using Enzo IL-6 (mouse) ELISA kit (Enzo Life Sciences, ADI-900–045), according to manufacturer's instructions. IFNγ quantification was performed in protein samples (prepared as for western blot analysis) diluted 1:20 using Abcam IFNγ (mouse) ELISA kit (Abcam, ab46081), according to manufacturer's instructions. IL-6 and IFNγ content was normalized to protein content for all samples and quantifications are shown as pg/ mg protein.

Quantification of 4-HNE adducts in WAT extracts

4-HNE protein adducts were quantified in undiluted protein samples (prepared as for western blot analysis) using Cell Biolabs Oxiselect HNE Adduct competitive ELISA kit (Cell Biolabs, Inc., STA-838), according to manufacturer's instructions. 4-HNE content was normalized to protein content for all samples and quantifications are shown as μg/ mg protein.

Statistical Analysis

All data are presented as average and standard error of mean (s.e.m.). Statistical analysis was carried out using Microsoft Excel or GraphPad Prism 5. For comparisons between two groups, two-tailed Student's t-test was used to determine statistical significance, assuming normal distribution and equal variance. For multiple comparisons, one-way ANOVA with Dunnett's multiple comparison post-test or Bonferroni's multiple comparison post-test were used to determine statistical significance. For fly demographics, statistical analysis was carried out using GraphPad Prism 5.

Supplementary Material

Refer to Web version on PubMed Central for supplementary material.

Acknowledgments

We thank Mia Konjikusic for technical help with the mouse colony, Andrea Ireland and Margeret Ray from Calico Labs for help with library preparation and RNA Sequencing and Dr. Huifei Liu for providing an expert pathologist evaluation of liver sections. Work in Dr. Jasper's lab is supported by NIH grants AG052989, AG050104 and AG047497 and some work was supported by Calico Labs. Work in Dr. Lamba's lab is supported by NIH grant EY025779. Work in Dr. Villeda's lab is supported by NIH grant AG055797. Dr. Sousa-Victor and Dr. Neves are supported by the Glenn Foundation for Medical Research

References

1. Lopez-Otin C, Blasco MA, Partridge L, Serrano M & Kroemer G The hallmarks of aging. Cell 153, 1194–1217 (2013). [PubMed: 23746838]
2. Franceschi C, et al. Inflamm-aging. An evolutionary perspective on immunosenescence. Annals of the New York Academy of Sciences 908, 244–254 (2000). [PubMed: 10911963]
3. Villeda SA, et al. The ageing systemic milieu negatively regulates neurogenesis and cognitive function. Nature 477, 90–94 (2011). [PubMed: 21886162]
4. Smith LK, et al. beta2-microglobulin is a systemic pro-aging factor that impairs cognitive function and neurogenesis. Nature medicine 21, 932–937 (2015).
5. Conboy IM, et al. Rejuvenation of aged progenitor cells by exposure to a young systemic environment. Nature 433, 760–764 (2005). [PubMed: 15716955]
6. Rebo J, et al. A single heterochronic blood exchange reveals rapid inhibition of multiple tissues by old blood. Nature communications 7, 13363 (2016).
7. Ruckh JM, et al. Rejuvenation of regeneration in the aging central nervous system. Cell stem cell 10, 96–103 (2012). [PubMed: 22226359]
8. Murray PJ & Wynn TA Protective and pathogenic functions of macrophage subsets. Nature reviews. Immunology 11, 723–737 (2011).
9. Miron VE, et al. M2 microglia and macrophages drive oligodendrocyte differentiation during CNS remyelination. Nature neuroscience 16, 1211–1218 (2013). [PubMed: 23872599]
10. Li H, Qi Y & Jasper H Preventing Age-Related Decline of Gut Compartmentalization Limits Microbiota Dysbiosis and Extends Lifespan. Cell host & microbe 19, 240–253 (2016). [PubMed: 26867182]
11. Clark RI & Walker DW Role of gut microbiota in aging-related health decline: insights from invertebrate models. Cellular and molecular life sciences : CMLS (2017).
12. Clark RI, Walker DW & Dionne MS Metabolic and immune integration in aging and age-related disease. Aging 6, 3–4 (2014). [PubMed: 24399758]
13. Barzilai N, Huffman DM, Muzumdar RH & Bartke A The critical role of metabolic pathways in aging. Diabetes 61, 1315–1322 (2012). [PubMed: 22618766]
14. Gan L, Chitturi S & Farrell GC Mechanisms and implications of age-related changes in the liver: nonalcoholic Fatty liver disease in the elderly. Current gerontology and geriatrics research 2011, 831536 (2011). [PubMed: 21918648]
15. Sheedfar F, Di Biase S, Koonen D & Vinciguerra M Liver diseases and aging: friends or foes? Aging cell 12, 950–954 (2013). [PubMed: 23815295]
16. Park JH, et al. Daumone fed late in life improves survival and reduces hepatic inflammation and fibrosis in mice. Aging cell 13, 709–718 (2014). [PubMed: 24796965]
17. Larsen CM, et al. Interleukin-1-receptor antagonist in type 2 diabetes mellitus. The New England journal of medicine 356, 1517–1526 (2007). [PubMed: 17429083]
18. Donath MY & Shoelson SE Type 2 diabetes as an inflammatory disease. Nature reviews. Immunology 11, 98–107 (2011).
19. Neves J, et al. Immune modulation by MANF promotes tissue repair and regenerative success in the retina. Science 353, aaf3646 (2016). [PubMed: 27365452]
20. Lindholm P & Saarma M Novel CDNF/MANF family of neurotrophic factors. Developmental neurobiology 70, 360–371 (2010). [PubMed: 20186704]
21. Galli E, et al. Increased circulating concentrations of mesencephalic astrocyte-derived neurotrophic factor in children with type 1 diabetes. Scientific reports 6, 29058 (2016). [PubMed: 27356471]
22. Wu T, et al. Circulating mesencephalic astrocyte-derived neurotrophic factor is increased in newly diagnosed prediabetic and diabetic patients, and is associated with insulin resistance. Endocrine journal 64, 403–410 (2017). [PubMed: 28216543]
23. Lindholm P, et al. MANF is widely expressed in mammalian tissues and differently regulated after ischemic and epileptic insults in rodent brain. Molecular and cellular neurosciences 39, 356–371 (2008). [PubMed: 18718866]

24. Lindahl M, Saarma M & Lindholm P Unconventional neurotrophic factors CDNF and MANF: Structure, physiological functions and therapeutic potential. Neurobiology of disease 97, 90–102 (2017). [PubMed: 27425895]
25. Voutilainen MH, et al. Mesencephalic astrocyte-derived neurotrophic factor is neurorestorative in rat model of Parkinson's disease. The Journal of neuroscience : the official journal of the Society for Neuroscience 29, 9651–9659 (2009). [PubMed: 19641128]
26. Chen L, et al. Mesencephalic astrocyte-derived neurotrophic factor is involved in inflammation by negatively regulating the NF-kappaB pathway. Scientific reports 5, 8133 (2015). [PubMed: 25640174]
27. Yang S, Huang S, Gaertig MA, Li XJ & Li S Age-dependent decrease in chaperone activity impairs MANF expression, leading to Purkinje cell degeneration in inducible SCA17 mice. Neuron 81, 349–365 (2014). [PubMed: 24462098]
28. Glass D, et al. Gene expression changes with age in skin, adipose tissue, blood and brain. Genome biology 14, R75 (2013). [PubMed: 23889843]
29. Ayyaz A & Jasper H Intestinal inflammation and stem cell homeostasis in aging Drosophila melanogaster. Frontiers in cellular and infection microbiology 3, 98 (2013). [PubMed: 24380076]
30. Yang S, et al. MANF regulates hypothalamic control of food intake and body weight. Nature communications 8, 579 (2017).
31. Lindahl M, et al. MANF is indispensable for the proliferation and survival of pancreatic beta cells. Cell reports 7, 366–375 (2014). [PubMed: 24726366]
32. Schmucker DL Age-related changes in liver structure and function: Implications for disease? Experimental gerontology 40, 650–659 (2005). [PubMed: 16102930]
33. Rabinowitz SS & Gordon S Macrosialin, a macrophage-restricted membrane sialoprotein differentially glycosylated in response to inflammatory stimuli. The Journal of experimental medicine 174, 827–836 (1991). [PubMed: 1919437]
34. Kinoshita M, et al. Characterization of two F4/80-positive Kupffer cell subsets by their function and phenotype in mice. Journal of hepatology 53, 903–910 (2010). [PubMed: 20739085]
35. Walker DG & Lue LF Immune phenotypes of microglia in human neurodegenerative disease: challenges to detecting microglial polarization in human brains. Alzheimer's research & therapy 7, 56 (2015).
36. Oishi Y & Manabe I Macrophages in age-related chronic inflammatory diseases. NPJ aging and mechanisms of disease 2, 16018 (2016). [PubMed: 28721272]
37. Baker DJ, et al. Naturally occurring p16(Ink4a)-positive cells shorten healthy lifespan. Nature 530, 184–189 (2016). [PubMed: 26840489]
38. Higami Y, et al. Aging accelerates but life-long dietary restriction suppresses apoptosis-related Fas expression on hepatocytes. The American journal of pathology 151, 659–663 (1997). [PubMed: 9284813]
39. Gregg SQ, et al. A mouse model of accelerated liver aging caused by a defect in DNA repair. Hepatology 55, 609–621 (2012). [PubMed: 21953681]
40. Le Couteur DG, et al. The Aging Liver and the Effects of Long Term Caloric Restriction in Restriction Calorie, Aging and Longevity (eds. Everitt A, Rattan S, le Couteur D & de Cabo R) pp 191–216 (Springer, Dordrecht, 2010).
41. Yang L, Yang L, Dong C & Li L The class D scavenger receptor CD68 contributes to mouse chronic liver injury. Immunologic research 66, 414–424 (2018). [PubMed: 29804196]
42. Stahl EC & Brown BN Kupffer cell subsets differ between young and aged murine livers. J Immunol 196 (Supplement 126131) (2016).
43. Gordon S Alternative activation of macrophages. Nature reviews. Immunology 3, 23–35 (2003).
44. Singh P, et al. Lymphoid neogenesis and immune infiltration in aged liver. Hepatology 47, 1680–1690 (2008). [PubMed: 18395842]
45. White RR, et al. Comprehensive transcriptional landscape of aging mouse liver. BMC genomics 16, 899 (2015). [PubMed: 26541291]
46. Bataller R & Brenner DA Liver fibrosis. The Journal of clinical investigation 115, 209–218 (2005). [PubMed: 15690074]

47. Warren A, et al. The effects of old age on hepatic stellate cells. Current gerontology and geriatrics research 2011, 439835 (2011). [PubMed: 21687587]
48. Palgi M, Greco D, Lindstrom R, Auvinen P & Heino TI Gene expression analysis of Drosophilaa Manf mutants reveals perturbations in membrane traffic and major metabolic changes. BMC genomics 13, 134 (2012). [PubMed: 22494833]
49. Heckmann BL, Zhang X, Xie X & Liu J The G0/G1 switch gene 2 (G0S2): regulating metabolism and beyond. Biochimica et biophysica acta 1831, 276–281 (2013). [PubMed: 23032787]
50. Yang X, et al. The G(0)/G(1) switch gene 2 regulates adipose lipolysis through association with adipose triglyceride lipase. Cell metabolism 11, 194–205 (2010). [PubMed: 20197052]
51. Jung S, et al. Analysis of fractalkine receptor CX(3)CR1 function by targeted deletion and green fluorescent protein reporter gene insertion. Molecular and cellular biology 20, 4106–4114 (2000). [PubMed: 10805752]
52. Auffray C, et al. Monitoring of blood vessels and tissues by a population of monocytes with patrolling behavior. Science 317, 666–670 (2007). [PubMed: 17673663]
53. Castellano JM, et al. Human umbilical cord plasma proteins revitalize hippocampal function in aged mice. Nature 544, 488–492 (2017). [PubMed: 28424512]
54. Sato S, et al. Circadian Reprogramming in the Liver Identifies Metabolic Pathways of Aging. Cell 170, 664–677 e611 (2017). [PubMed: 28802039]
55. Kanfi Y, et al. The sirtuin SIRT6 regulates lifespan in male mice. Nature 483, 218–221 (2012). [PubMed: 22367546]
56. Swindell WR Genes and gene expression modules associated with caloric restriction and aging in the laboratory mouse. BMC genomics 10, 585 (2009). [PubMed: 19968875]
57. Houtkooper RH, et al. The metabolic footprint of aging in mice. Scientific reports 1, 134 (2011). [PubMed: 22355651]
58. Elabd C, et al. Oxytocin is an age-specific circulating hormone that is necessary for muscle maintenance and regeneration. Nature communications 5, 4082 (2014).
59. Loffredo FS, et al. Growth differentiation factor 11 is a circulating factor that reverses age-related cardiac hypertrophy. Cell 153, 828–839 (2013). [PubMed: 23663781]
60. Zhang G, et al. Hypothalamic programming of systemic ageing involving IKK-beta, NF-kappaB and GnRH. Nature 497, 211–216 (2013). [PubMed: 23636330]
61. Neves J, Sousa-Victor P & Jasper H Rejuvenating Strategies for Stem Cell-Based Therapies in Aging. Cell stem cell 20, 161–175 (2017). [PubMed: 28157498]
62. Malhi H & Kaufman RJ Endoplasmic reticulum stress in liver disease. Journal of hepatology 54, 795–809 (2011). [PubMed: 21145844]
63. Wang Y, et al. The g0/g1 switch gene 2 is an important regulator of hepatic triglyceride metabolism. PloS one 8, e72315 (2013). [PubMed: 23951308]
64. Sugaya Y & Satoh H Liver-specific G0 /G1 switch gene 2 (G0s2) expression promotes hepatic insulin resistance by exacerbating hepatic steatosis in male Wistar rats. Journal of diabetes 9, 754–763 (2017). [PubMed: 27624922]
65. Heckmann BL, et al. Liver X receptor alpha mediates hepatic triglyceride accumulation through upregulation of G0/G1 Switch Gene 2 expression. JCI insight 2, e88735 (2017). [PubMed: 28239648]
66. Huang SC, et al. Cell-intrinsic lysosomal lipolysis is essential for alternative activation of macrophages. Nature immunology 15, 846–855 (2014). [PubMed: 25086775]
67. Day CP Pathogenesis of steatohepatitis. Best practice & research. Clinical gastroenterology 16, 663–678 (2002). [PubMed: 12406438]
68. Fontana L, et al. Aging promotes the development of diet-induced murine steatohepatitis but not steatosis. Hepatology 57, 995–1004 (2013). [PubMed: 23081825]
69. Yavarna T, et al. High diagnostic yield of clinical exome sequencing in Middle Eastern patients with Mendelian disorders. Human genetics 134, 967–980 (2015). [PubMed: 26077850]
70. Sousa-Victor P, et al. Geriatric muscle stem cells switch reversible quiescence into senescence. Nature 506, 316–321 (2014). [PubMed: 24522534]

71. Parkhurst CN, et al. Microglia promote learning-dependent synapse formation through brain-derived neurotrophic factor. Cell 155, 1596–1609 (2013). [PubMed: 24360280]

72. Villeda SA, et al. Young blood reverses age-related impairments in cognitive function and synaptic plasticity in mice. Nature medicine 20, 659–663 (2014).

73. Sun Z, et al. Hepatic Hdac3 promotes gluconeogenesis by repressing lipid synthesis and sequestration. Nature medicine 18, 934–942 (2012).

74. Liu F, Song Y & Liu D Hydrodynamics-based transfection in animals by systemic administration of plasmid DNA. Gene therapy 6, 1258–1266 (1999). [PubMed: 10455434]

75. Tiscornia G, Singer O & Verma IM Production and purification of lentiviral vectors. Nature protocols 1, 241–245 (2006). [PubMed: 17406239]

76. Huang da W., Sherman BT & Lempicki RA Systematic and integrative analysis of large gene lists using DAVID bioinformatics resources. Nature protocols 4, 44–57 (2009). [PubMed: 19131956]

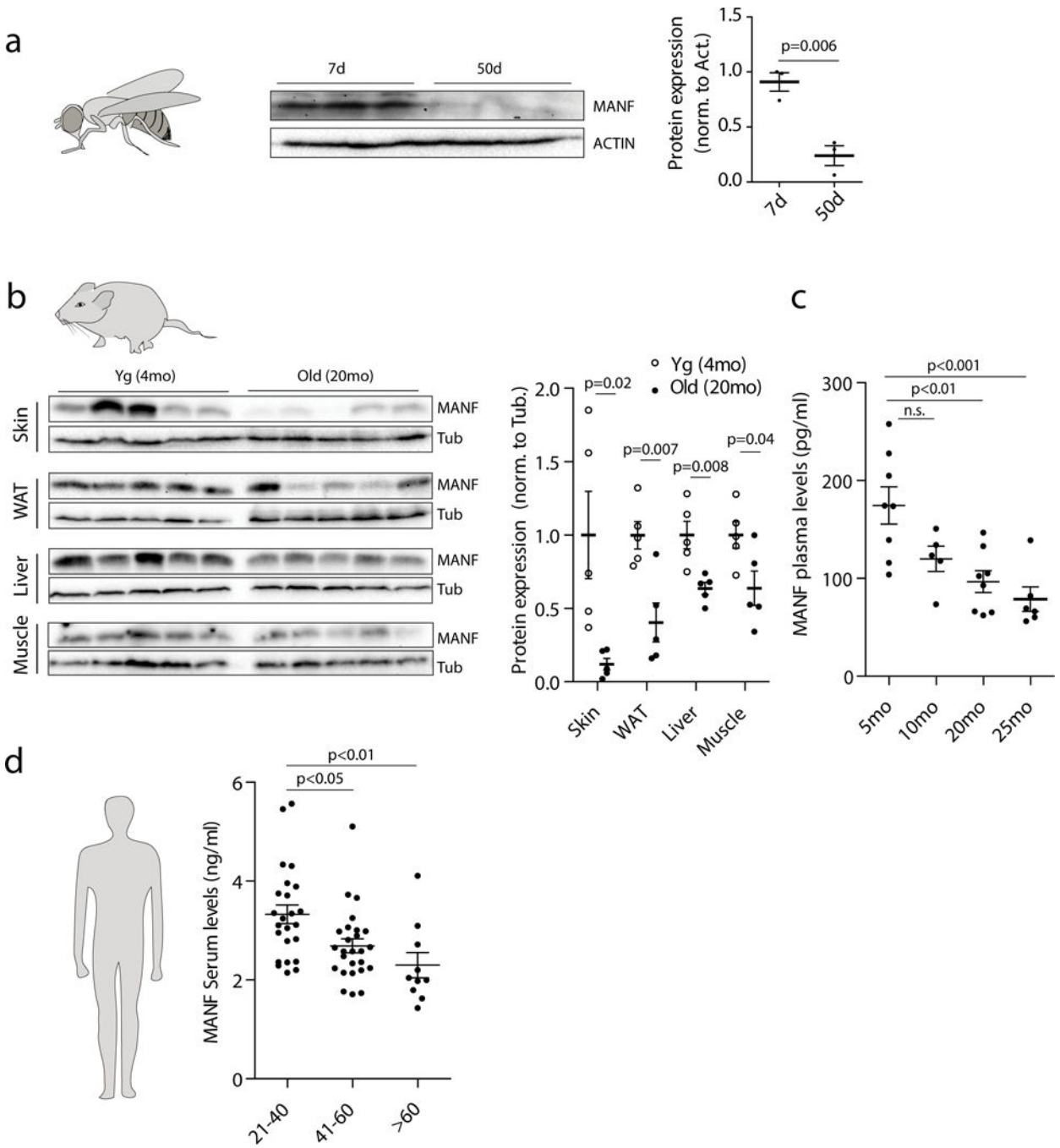

Figure 1. MANF protein levels decline with age in flies, mice and humans.

a, Western blot analysis of MANF levels in protein extracts of WT (W^{1118}) whole flies, 7 and 50 days old. Quantification of relative average levels of MANF, normalized to actin levels, are represented (n=3 samples/age, 5 flies/sample). **b,** Western blot analysis of MANF levels in protein extracts from different tissues of 4 month old and 20 month old WT (C57BL/6JN) mice. Quantification of relative average levels of MANF, normalized to tubulin levels, are represented for each tissue at each age (n=5/condition). **c,** MANF protein levels in plasma of WT (C57BL/6JN) mice (n=5, 10mo; n=6, 25mo; n=8, 5mo and 20mo),

quantified by ELISA. **d,** MANF protein levels in human serum (n=24, age 21–40; n=26, age 41–69, n=10 age >60), quantified by ELISA. Data are represented as average ± s.e.m and each n represents one animal/human subject. In a and b, p values are from two-tailed Student's t-test. In c and d, p values are from one-way ANOVA with Dunnett's multiple comparison post-test. Full blots for a and b can be found in Supplementary Figure 11.

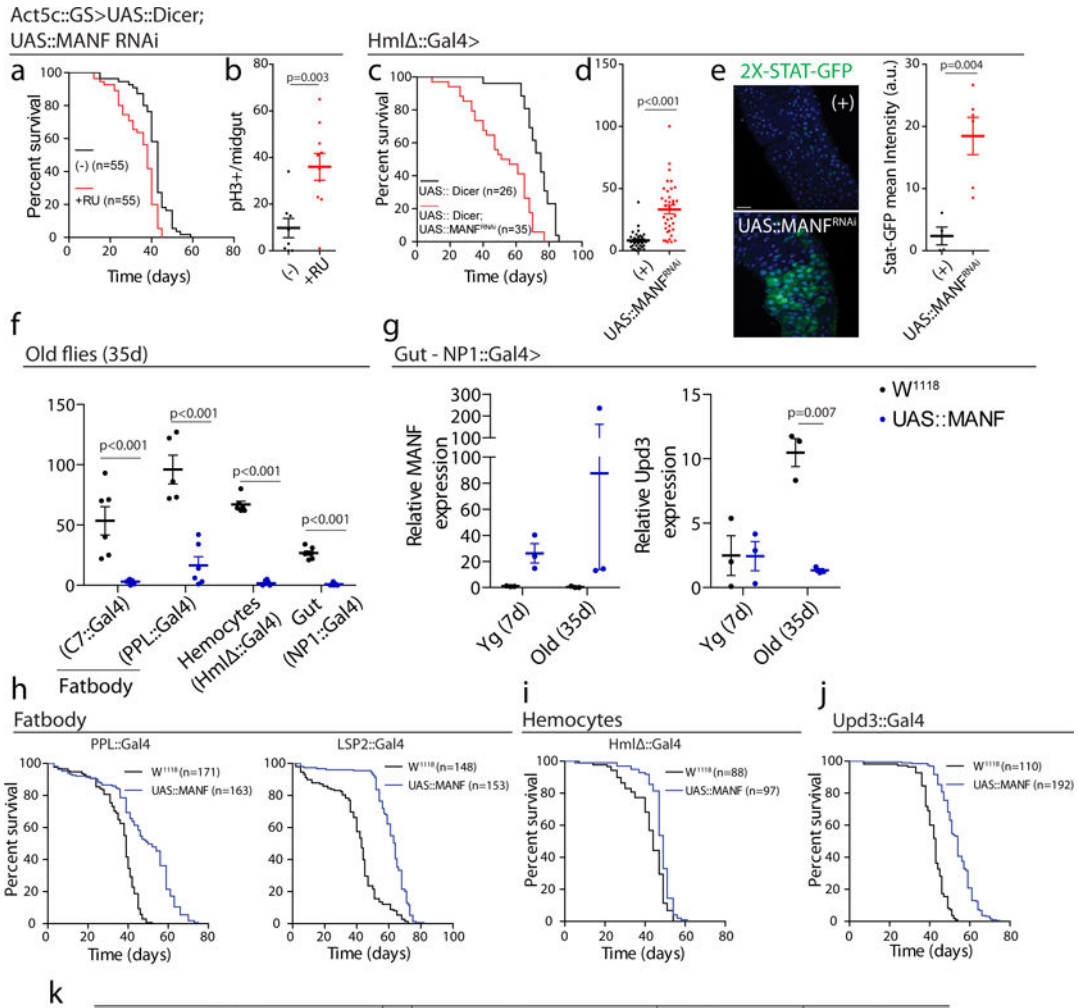

k

Condition			Lifespan				Chi-square		p-value	
Genotype	RU 486	N	median	%change	max	%change	Mantel-Cox	Wilcoxon	Mantel-Cox	Wilcoxon
Act5cGS; UAS::Dicer2; UAS::MANFRNAi	-	2	43	-11.628%	59	-23.729%	22.96	20.12	< 0.0001	< 0.0001
	+	2	38		45					
HmlΔGal4; UAS::Dicer2 HmlΔGal4; UAS::Dicer2; UAS::MANFRNAi	-	2	75	-28.000%	86	-10.465%	25.45	24.08	< 0.0001	< 0.0001
	-	2	54		77					
PPLGal4/+ PPLGal4/UAS::MANF	-	6	39	28.205%	52	48.077%	108.5	63.76	< 0.0001	< 0.0001
	-	6	50		77					
LSP2Gal4/+ LSP2Gal4/UAS::MANF	-	7	43	48.837%	72	13.889%	139.1	152	< 0.0001	< 0.0001
	-	7	64		82					
HmlΔGal4/+ HmlΔGal4/UAS::MANF	-	3	44	11.364%	54	12.963%	21.36	24.86	< 0.0001	< 0.0001
	-	3	49		61					
Upd3Gal4/+ Upd3Gal4/UAS::MANF	-	5	43	25.581%	54	38.889%	185.8	169.5	< 0.0001	< 0.0001
	-	7	54		75					
ElavGal4/+ ElavGal4/UAS::MANF	-	3	57	-12.281%	78	5.128%	7.889	24.35	0.005	< 0.0001
	-	3	50		82					

Figure 2. MANF overexpression extends lifespan in *Drosophila*

a,c, Demographics of flies expressing MANF-RNAi under the control of ubiquitous (Act5c::GS, a) or hemocyte specific (HmlΔ::Gal4, c) drivers. All flies are female and fly numbers (n) are indicated for each genotype or treatment. **b,d,** Quantification of mitotic figures (pH3+ cells) in midguts of flies expressing MANF-RNAi under the control of ubiquitous (b, Act5c::GS: n=8 guts, (−); n=10 guts, +RU) or hemocyte specific (d, HmlΔ::Gal4,=: n=33 guts, UAS::Dicer; n=36 guts, UAS::Dicer,UAS::MANF^{RNAi}) drivers for 14 days and 7 days, respectively. **e,** Representative images showing GFP expression

driven by a STAT reporter in midguts of flies expressing MANF-RNAi under the control of a hemocyte specific driver (HmlΔ::Gal4) for 7 days. Scale bar: 20μm. Quantification of average GFP-intensity/midgut is shown (n=4 guts, UAS::Dicer; n=6 guts, UAS::Dicer,UAS::MANF^{RNAi}). **f,** Quantification of mitotic figures (pH3+ cells) in midguts of 35 day old flies overexpressing MANF under the control of different drivers (n=5 guts, w^{1118}: PPL::Gal4; n=6 guts, w^{1118}: C7::Gal4 and Hml::Gal4 and UAS::MANF: PPL::Gal4; n=7 guts, w^{1118}: NP1::Gal4 and UAS::MANF: C7::Gal4 and NP1::Gal4; n=8 guts, UAS::MANF: Hml::Gal4). **g,** Relative levels of MANF and Upd3 transcripts, quantified by RT-qPCR, in midguts of 35 day old flies overexpressing MANF in enterocytes (n=3/age and genotype, each n represents a pool of 8 guts). **h-j,** Demographics of flies overexpressing MANF in fatbody (PPL::Gal4 and LSP2::Gal4, h), hemocytes (HmlΔ::Gal4, i) or in tissues that express Upd3 (Upd3::Gal4, j). All flies are female and fly numbers (n) are indicated for each genotype. **k,** Statistical analysis of lifespan experiments in a,c,h,i,j. N represents the number of independent populations pooled in each lifespan graph. The number of animals (n) used to generate each lifespan graph, and for statistical analysis, are indicated in the corresponding graph. For b,d,e,f,g data are represented as average ± s.e.m. and p values are from two-tailed Student's t-test.

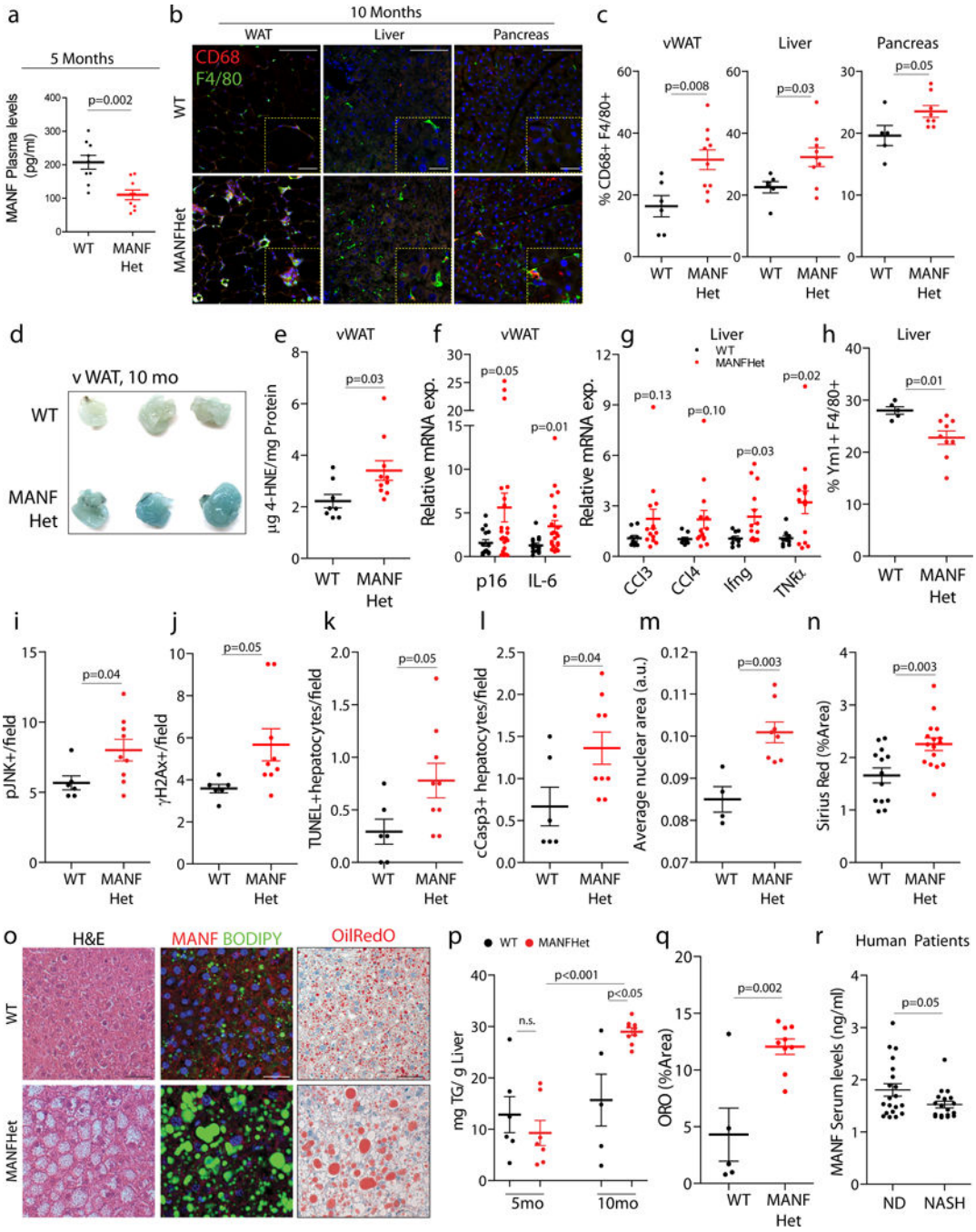

Figure 3. Mice with reduced MANF levels develop inflammation and liver damage.

a, MANF protein levels in plasma of 5 month old MANFHet mice or WT littermates (n=9/condition). **b,** Representative images from 10 month old MANFHet mice, or WT littermates, immunostained against F4/80 (green) and CD68 (red). Scale bars: WAT, 200µm, 50µm inset; liver and pancreas, 100µm, 25µm inset. Quantifications of these stainings, for independent animals, are shown in Fig. 3c and Supplementary Fig. 2c. **c,** Quantification of the average number of activated macrophages in 10 month old MANFHet mice, or WT littermates (vWAT: n=6, WT, n=10, MANFHet; Liver: n=6, WT, n=9, MANFHet; Pancreas: n=5, WT,

n=8, MANFHet). **d,** SA-βGal staining in vWAT of 10 month old MANFHet mice, or WT littermates. These observations were reproduced in two sets of animals with a total n=9/WT and n=10/MANFHet mice. **e-g,** Quantification of 4-HNE adducts in protein extracts from vWAT (e, n=8, WT; n=10, MANFHet) and relative expression, quantified by RT-qPCR, in vWAT (f, n=15, WT; n=22, MANFHet) or livers (g, n=9, WT; n=14, MANFHet) of 10 month old MANFHet mice, or WT littermates. **h-m,** Quantification of the average %Ym1+ cells (h), the average number of p-JNK+ cells (i), γH2Ax+ cells (j), TUNEL+ hepatocytes (k), cleaved-caspase3+ hepatocytes (l) and nuclear area (m) in livers of 10 month old MANFHet mice, or WT littermates (n=5, WT; n=9, MANFHet, see Supplementary Fig. 2e,l for representative images). **n,** Collagen deposition in livers of 10 month old MANFHet mice and WT littermates, quantified as the percentage of area occupied by Sirius Red stain (n=13, WT; n=16, MANFHet, see Supplementary Fig. 2m for representative images). **o,** Representative images stained with hematoxylin and eosin (H&E, left), immunostained against MANF (red) and co-stained with Bodipy (green, middle), or stained with OilRedO (right), from livers of 10 month old MANFHet mice, or WT littermates. Scale bars: 50μm. Quantifications of these stainings, for independent animals, are shown in Fig. 3q and Supplementary Fig. 4d. **p,q,** Fat content in livers of MANFHet mice and WT littermates, quantified as triglyceride content (p) or as the percentage of area occupied by OilRedO stain (q). 5mo: n=6, WT; n=7, MANFHet; 10mo: n=5, WT; n=9, MANFHet. **r,** MANF protein levels in human serum from NASH patients (n=18) and non-diseased age-matched subjects (ND, n=20). Data are represented as average ± s.e.m. and each n represents one animal. In a,c,e-n,q,r, p values are from two-tailed Student’s t-test. In p, p values are from one-way ANOVA with Bonferroni’s multiple comparison post-test.

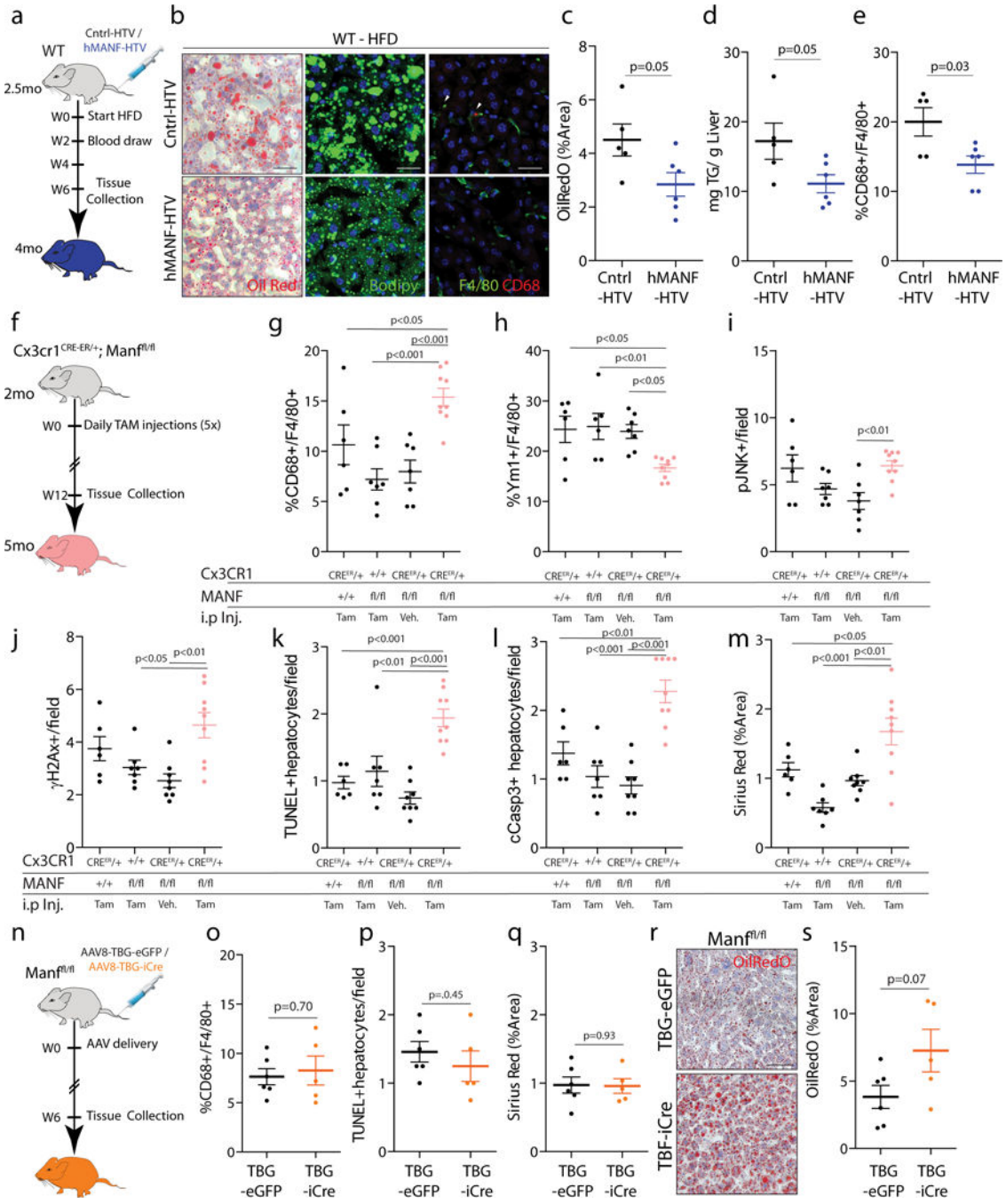

Figure 4. Immune cell-derived MANF and hepatocyte-derived MANF contribute to liver homeostasis.

a, Experimental timeline for analysis of animals fed HFD for 6 weeks after receiving hydrodynamic tail vein (HTV) injections of plasmids expressing hMANF. **b,** Representative images of cryosections from livers of 4 month old WT (C57BL/6JN) mice fed HFD for 6 weeks after receiving hMANF HTV injections, stained with OilRedO (left), Bodipy (middle), or immunostained against F4/80 (green, right) and CD68 (red, right). DAPI is used to identify nuclei. Scale bars: 50μm. Quantifications of these stainings, for independent

animals, are shown in Fig. 4c,e and Supplementary Fig. 5e. **c-e,** Quantification of fat content, as the percentage of area occupied by OilRedO stain (c), triglyceride content (d) and the average number of activated macrophages as the %CD68+ cells within the F4/80+ population (e) in livers of 4 month old WT mice fed HFD for 6 weeks after receiving hMANF HTV injections (n=5, Cntrl-HTV; n=6, hMANF-HTV). **f,** Experimental timeline for analysis of animals with conditional ablation of MANF in Cx3cr1-expressing monocytes/macrophages. **g-m,** Quantification of the average number of activated macrophages as the %CD68+ cells within the F4/80+ population (g), %Ym1+ cells within the F4/80+ population (h), p-JNK+ cells (i), γH2Ax+ cells (j), TUNEL+ hepatocytes (k), cleaved caspase3+ hepatocytes (l) and collagen deposition, as the percentage of area occupied by Sirius Red stain (m) in livers of $Cx3cr1^{CRE-ER/+}$,$MANF^{fl/fl}$ mice, 12 weeks after tamoxifen treatment (n=6, Cre^{ER} +Tam; n=7, $Manf^{fl/fl}$ +Tam; n=8, $Cre^{ER}/Manf^{fl/fl}$ +Veh.; n=9, $Cre^{ER}/Manf^{fl/fl}$ +Tam, see Supplementary Fig. 5g for representative images for each condition). **n,** Experimental timeline for analysis of animals with conditional ablation of MANF in hepatocytes. **o-q,s,** Quantification of the average number of activated macrophages as the %CD68+ cells within the F4/80+ population (o), TUNEL+ hepatocytes (p), collagen deposition, as the percentage of area occupied by Sirius Red stain (q) and fat content, as the percentage of area occupied by OilRedO stain (s), in livers of $MANF^{fl/fl}$ mice, 6 weeks after injection with AAV-TBGi-Cre (n=6, TBG-eGFP; n=5, TBG-iCre). **r,** Representative images of cryosections from livers of $MANF^{fl/fl}$ mice, 6 weeks after injection with AAV-TBGi-Cre, stained with OilRedO. Scale bar: 50μm. Quantifications of these stainings, for independent animals, are shown in Fig. 4s. Data are represented as average ± s.e.m. and each n represents one animal. In c-e,o-q,s, p values are from two-tailed Student's t-test. In g-m, p values are from one-way ANOVA with Dunnett's multiple comparison post-test.

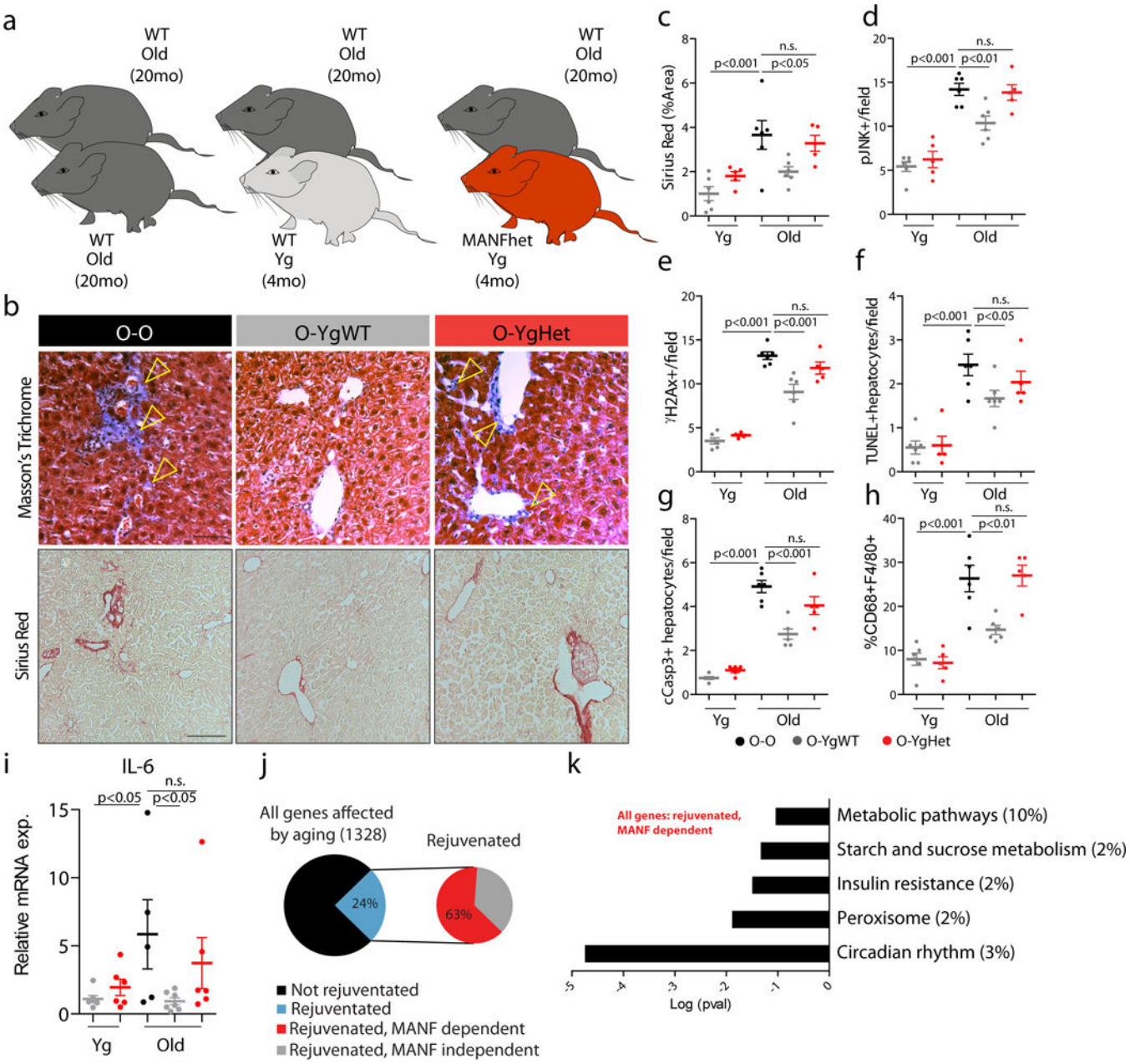

Figure 5. MANF is required for full liver rejuvenation by heterochronic parabiosis.

a, Experimental setup for the mouse pairs used in the heterochronic parabiosis experiment. In b-i animals from O-O pairs are represented in black, animals from O-YgWT pairs are represented in grey and animals from O-YgHet pairs are represented in red. **b,** Representative images of Masson's trichrome stain in paraffin sections (Scale bar: 50μm) and Sirius Red stain in cryosections (Scale bar: 200μm) from livers of old animals of each parabiosis pair type. Arrowheads indicate collagen deposition. Quantifications of these stainings, for independent animals, are shown in Fig. 5c. **c-h,** Quantification of collagen deposition, as the percentage of area occupied by Sirius Red stain (c), the average number of p-JNK+ cells (d), γH2Ax+ cells (e), TUNEL+ hepatocytes (f), cleaved caspase3+

hepatocytes (g) and activated macrophages, as the %CD68+ cells within the F4/80+ population (h) in livers of young and old animals from each parabiosis pair type (n=5, O-Yg Het; n=6, O-O and O-Yg WT, see Supplementary Fig. 6b for representative images for each condition). **i,** Relative levels of IL-6 transcripts, quantified by RT-qPCR, in livers of young and old animals from each parabiosis pair type (n=5, O-O; n=6, O-Yg Het; n=7, O-Yg WT). **j,** Pie chart representing the percentage of genes affected by aging in the liver (left pie chart) rejuvenated by heterochronic parabiosis (blue on left pie chart and whole pie chart on right) in a MANF-dependent manner (red on right pie chart), n=5/condition. See also Supplementary Fig. 6h. k, Graph showing significantly enriched KEGG pathways in the dataset of liver genes affected by aging and rejuvenated by heterochronic parabiosis in a MANF-dependent manner, n=5/condition. Percentage of genes in the dataset belonging to each KEGG pathway is indicated. See also Supplementary Fig. 6i. Data are represented as average ± s.e.m. and each n represents one animal. In c-i, p values are from one-way ANOVA with Dunnett's multiple comparison post-test. In k, p values are from Fisher Exact test.

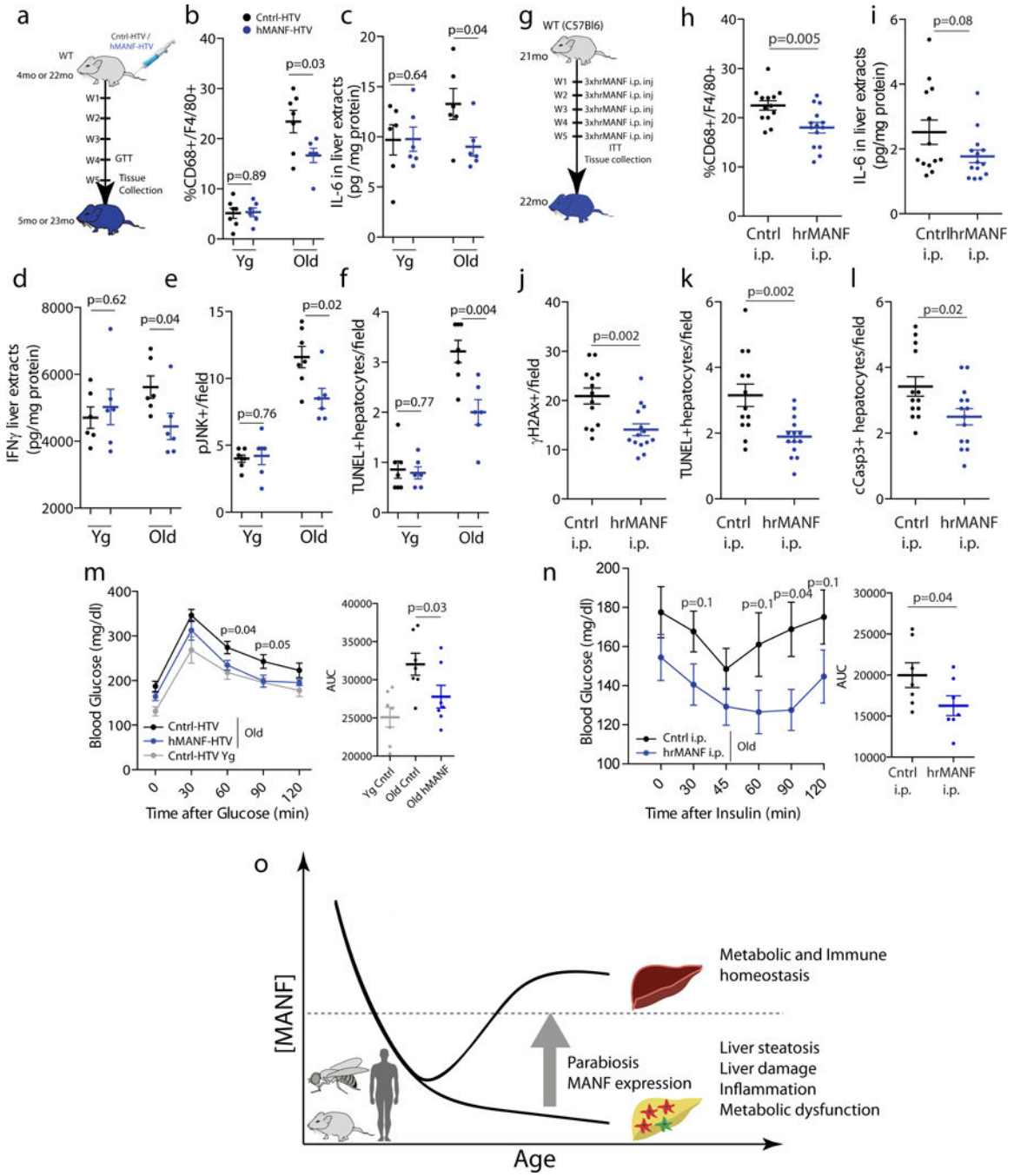

Figure 6. MANF improves liver damage, inflammation and metabolic dysfunction in old mice.

a, Experimental timeline for analysis of young and old animals, after receiving HTV injections of plasmids expressing hMANF. **b,e,f,** Quantification of the average number of activated macrophages as the %CD68+ cells within the F4/80+ population (b), p-JNK+ cells (e) and TUNEL+ hepatocytes (f) in livers of young and old WT mice, 5 weeks after receiving hMANF HTV injections (n=7, Cntrl-HTV, n=6, hMANF-HTV, see Supplementary Fig. 7c,e for representative images for each condition). **c,d,** IL-6 (c) and IFNγ (d) levels in protein samples from livers of young and old WT mice, 5 weeks after receiving hMANF

HTV injections, quantified by ELISA (n=6/condition). **g,** Experimental timeline for analysis of old animals, after 5 weeks treatment with hrMANF protein intra peritoneal injections. **h,j-l,** Quantification of the average number of activated macrophages as the %CD68+ cells within the F4/80+ population (h), γH2Ax+ cells (j), TUNEL+ hepatocytes (k) and cleaved caspase3+ hepatocytes (l) in livers of old WT mice, 5 weeks after receiving hrMANF i.p injections (n=13, Cntrl. i.p.; n=14, hrMANF i.p., see Supplementary Fig. 8c for representative images for each condition). **i,** IL-6 levels in protein samples from livers of old WT mice, 5 weeks after receiving hrMANF i.p injections, quantified by ELISA (n=13, Cntrl. i.p.; n=14, hrMANF i.p.). **m,** Glucose tolerance test of young and old WT mice, 4 weeks after receiving hMANF HTV injections. Graph represents average glucose levels in blood at the designated times after i.p. injections of glucose. p values shown are for differences between hMANF and control injections in old animals at the designated time points (n=7/condition). Graph to the right represents the average area under the curve (AUC) for each condition. **n,** Insulin tolerance test of old WT mice, 5 weeks after receiving hrMANF i.p. injections. Graph represents average glucose levels in blood at the designated times after i.p. injections of insulin. p values shown are for differences between hrMANF and control injections in old animals at the designated time points (n=7/condition). Graph to the right represents the average area under the curve (AUC) for each condition. **o,** Proposed model for the anti-geronic function of MANF. Data are represented as average ± s.e.m. and each n represents one animal. p values are from two-tailed Student’s t-test.